COLLOIDAL DISKS, FABRICATION AND SELF-ASSEMBLING

ANDRES FERNANDO MEJIA MEJIA

UNIVERSIDAD INDUSTRIAL DE SANTANDER
FACULTAD DE INGENIERIAS FISICOQUÍMICAS
ESCUELA DE INGENIERÍA QUÍMICA
BUCARAMANGA
2008

COLLOIDAL DISKS, FABRICATION AND SELF-ASSEMBLING

ANDRES FERNANDO MEJIA MEJIA

Trabajo de Grado presentado como requisito para optar al título de Ingeniero Químico

Director

ZHENGDONG CHENG Ph.D

Texas A&M University

Lector

RAMIRO MARTINEZ REY Ph.D

Universidad Industrial de Santander

UNIVERSIDAD INDUSTRIAL DE SANTANDER
FACULTAD DE INGENIERIAS FISICOQUÍMICAS
ESCUELA DE INGENIERÍA QUÍMICA
BUCARAMANGA
2008

A mis padres Julio y Olga, los cuáles siempre me apoyaron en mis intenciones de ser Ingeniero Químico, me guiaron por el buen camino y me dieron una excelente educación en valores.

A mis hermanos Olga y Carlos, que siempre me pusieron un techo difícil de alcanzar, ya que mi meta fue al menos igualarlos, para mí, la gente más inteligente y capaz que yo he conocido.

A mi novia Carolina, la que siempre estuvo al lado mío durante toda mi vida universitaria, la que fue mi inspiración y me acompañó en los momentos felices y también difíciles.

A Paquita, por su fidelidad y por sus grandes muestras de cariño.

A mis amigos de la Universidad, sin su compañía jamás habría alcanzado lo que he logrado, nunca olvidaré las largas noches de estudio y las mamaderas de gallo.

Andrés Fernando Mejía Mejía

ACKNOWLEDGEMENTS

Al Doctor Zhengdong Cheng, el cuál fue mi tutor durante la elaboración de esta tesis, le quedo en deuda ante la oportunidad que recibí de parte de él de realizar esta pasantía, nunca olvidaré las largas horas de trabajo y como siempre creyó en mis facultades.

Al Doctor, Ramiro Martínez Rey, el cual siempre me apoyó incondicionalmente para la finalización de este proyecto de grado, su ánimo para la realización de la pasantía en Texas A&M y sus buenos consejos que me dió para la vida profesional.

A mis compañeros de grupo, Peng He, Srinivasa Pullela y a la Doctora Jingyi Shen, que en los momentos difíciles de este proyecto siempre estuvieron ahí para darme ánimos y sugerencias, además por ser tan incondicionales amigos.

Al Departamento de Ingeniería Química de la Universidad de Texas A&M y de la Universidad Industrial de Santander, los cuales me brindaron la oportunidad de realizar una pasantía en el extranjero que ayudó a ampliar mis conocimientos.

TABLE OF CONTENTS

Page.

LIST OF FIGURES

Page.

LIST OF TABLES

Page.

LIST OF ATTACHMENTS

Page.

ABSTRACT

TITLE: COLLOIDAL DISKS, FABRICATION AND SELF-ASSEMBLING*

AUTHOR: Andrés Fernando Mejía Mejía**

KEYWORDS: Polydispersity, Monodispersity, Electrospray, Emulsion, Surfactants, Liquid crystals, Sedimentation, Microdisks.

Monodisperse wax emulsions were prepared by electrospraying of melt wax. The size of the emulsions was tailored by varying physical parameters of the electrospray, such as the flow rate of the discontinuous phase, its electric conductivity, and the applied voltage. The monodispersity of the emulsions was greatly influenced by the surface tension and density of the collection liquid. We also demonstrated the fabrication of uniform wax microdisks using the phase transition of wax molecules inside these emulsions.

In the other hand, surfactants delicately tailor liquid/liquid interfaces which carry out a central part in many chemical, physical, and biological processes[1]. They are used as detergents[2-4], foam and emulsion stabilizers, surface modifier and droplet size controller for microfluidics[5-7], adjustors for the organization of liquid crystals[8, 9], growth regulators for nano particles[10, 11], and area maintainers for drop evaporation when making DNA chips[12]. Here, we demonstrate surfactants as shape transformer for colloids. They mold emulsions into microdisks via surface crystallization[13-15] at the alkene-water interface. Our experiments are the first application of surface freezing at hydrocarbon and water interface[14]. This interfacially controlled organization of molecules offers novel routes for soft material design, fabrication, and utilization.

The study of the liquid crystal of α-Eicosene had been performed by increasing the disks concentration by letting evaporate a coin like disks solution droplet and watching it through a polarizer light microscope. It formed a colorful domain which it was influenced by the disks concentration. In the red blood cell like disks case, the same experiment was done but with different conclusions, but, in spite of this, some color distribution was found, the molecular organization was not as good as the first one.

Finally, a sedimentation machine was used to study both discotic systems and a different phase transition had been found, with several conclusions about their different behavior.

---

*Proyecto de Grado desarrollado en Texas A&M University, College Station, Texas, USA.
**Facultad de Fisicoquímicas, Escuela de Ingeniería Química, Dir. Dr. Zhengdong Cheng, Lector: Dr. Ramiro Martínez Rey.

RESUMEN

TITULO: COLLOIDAL DISKS, FABRICATION AND SELF-ASSEMBLING*

AUTOR: Andrés Fernando Mejía Mejía**

PALABRAS CLAVES: Polidispersidad, Monodispersidad, Electrospray, Emulsión, Cristales Líquidos, Sedimentación, Microdiscos.

Emulsiones con micro partículas de α-Eicoseno fueron preparadas por el método del electrospray. El tamaño de las emulsiones fue controlado variando los parámetros físicos, como el flujo de la fase discontinua, su conductividad eléctrica y el voltaje aplicado al sistema. La monodispersidad de las emulsiones fue altamente influenciada por la tensión superficial y la densidad el líquido colector. Se fabricaron microdiscos uniformes de α-Eicoseno, conociendo y haciendo uso de la fase de transición de sus moléculas dentro de estas emulsiones.

Por otro lado, los surfactantes controlan minuciosamente las interfaces líquido/líquido que llevan a cabo gran parte de los procesos químicos, físicos y biológicos[1]. Ello son usados como detergentes[2-4], estabilizadores de espuma, emulsiones, modificadores de la superficie y para el control del tamaño de las gotas en los micro-fluidos [5-7], también sirven como supervisores para la organización de cristales líquidos [8, 9], reguladores de crecimiento de nano partículas [10, 11], y como agentes que mantienen el espacio para la evaporación de gotas cuando se fabrican chips de ADN [12].

En esta tesis, se demostró que los surfactantes funcionan como agentes reguladores de forma para coloides. Ellos moldean emulsiones en micro discos por medio de la cristalización de su superficie [13-15] en la interfase alcano-agua. Nuestros experimentos son la primera aplicación del 'surface freezing' en hidrocarbonos y la interfase del agua[14].

El estudio de formaciones de cristal líquido del α-Eicoseno también fueron evaluadas al permitir la evaporación de gotas con una emulsión de discos en forma de moneda (discos perfectos), mostrándonos perfectamente la distribución de una amplia gama de colores en función de la concentración de discos en la solución.

Finalmente, una máquina centrifugadora fue utilizada para estudiar ambos sistemas de discos. Diferentes fases de transición fueron encontradas, con conclusiones totalmente diferentes sobre su comportamiento.

---

*Proyecto de Grado desarrollado en Texas A&M University, College Station, Texas, USA.
**Facultad de Fisicoquímicas, Escuela de Ingeniería Química, Dir. Dr. Zhengdong Cheng, Lector: Dr. Ramiro Martínez Rey.

INTRODUCTION

Wax emulsions find wide applications in cosmetics[16], water proof paints[17, 18], adhesives[19], oil well fracturing[20], self-polishing emulsions for floor care[21], and fruit preservation[22]. They also can undergo phase transitions, interesting to us as examples of phase-change materials[23-25] and serving as model systems to investigate crystal nucleation and growth of hydrocarbons, polymers, surfactants, lipids, etc[26-29].

Here, we are interested in their shape transition[30] to fabricate discotic colloids. Colloids exist in a variety of shapes, such as spherical, rods, and disks. Among them, disks are the least studied and least explored despite their importance in many areas of research, such as petroleum (asphaltenes in the heavy oil are nano-disks)[31, 32], biology (red blood cells are microplatelets)[33] and agriculture (soils are aggregations of nano-disks)[34, 35]. Incomplete statistics by Lekkerkerker on papers presented on the 81st ACS Colloid and Surface Science Symposium showed that the study of sphere:rod:disk colloids are ~ 80:20:1. So far, a significant work has been carried out on micrometer-sized platelets[36-38], nanometer-sized disks in clay[39-42], synthetic clays[43-45] or nano-crystals[46], and lithographically fabricated particles[47-49]. There is a critical need to establish a model discotic colloidal system with uniform particle size of a few microns [50-56]. Current synthetic discotic colloidal systems often have a wide size distribution, as large as 17% [16, 18]. However, polydispersity has an important effect on the structure and phase transitions[57, 58]. A dispersion in particle size can suppress crystallization in hard sphere colloids[59]. In liquid crystals, polydispersity influences both the isotropic-nematic[60, 61] and the nematic-smectic[62, 63] transitions. Recent experiments demonstrated fractionation in thickness between the coexisting phases with the thicker platelets accumulating in the isotropic phase[64]. Insight into the dependence of liquid-crystal phases on the polydispersity in diameter and thickness of disks requires *further* study through experiment[38], theory and

simulations[65-67]. Mason et al.[30, 68] made disk-like wax particles by shearing hot α-Eicosene into a highly concentrated aqueous solution of SDS and lower the temperature to introduce shape change. A small portion of emulsions turned into a shape of thin circular cylindroids among others of variety of geometrical shapes. This experiment was the first hint of shape transition in phase changing colloids[23-25]. It intrigued us to investigate the drive forces for shape transition, including surfactant concentration and surface crystallization.

However it is hard to controls size and size distribution of the final particles obtained with this conventional emulsification method. Here, we seek ways of using electric field to produce uniform wax emulsions and hence to fabricate uniform colloidal disks.

The production of monodisperse aerosols using electrospray has been thoroughly studied[69-71] and extensively applied in many areas of science[72-77]. Loscertales and Marquez have shown the production of stable electrosprays in insulators baths[78] with the potential use for microencapsulation[79] and they have shown as well the process for this technology to be scale-up[80]. When a high electric field is applied to a liquid in a capillary, the liquid will form a conical meniscus[78] (**Fig. 1b**), through which a fine liquid ligament is ejected. The liquid ligament further breaks into a spray of droplets at downstream. The production of fine droplets is governed by the voltage applied to the capillary, the liquid flow rate and physical properties including the electric conductivity, surface tension, viscosity and dielectric constant of the liquid.

We produced uniform wax emulsions by emulsifying wax, using an electrospray. The entire process includes drop formation via electrospray and suspension formation via drop entrancement and stabilization in the ethanol aqueous solution. The emulsion droplets were further converted into disks by controlling the temperature.

In the other hand, once we got the discotic system, it helped us to study the anisotropic particles, which are model systems to study liquid crystals[36, 81]. So far, they are either taken directly from nature, such as filamentous viruses[82], DNA[83], microtubles[84], and minerals[85], or synthesis in the form of inorganic crystals[86, 87], polymeric colloids[88]. and lithographic particles [48, 49].

1. THEORY

1.1. EMULSIONS

Emulsion is a mixture of two immiscible liquids. They stay as two separate layers with a boundary between them. One liquid, the dispersed phase, will be dispersed in the other phase, the continuous phase. In our daily life, milk, mayonnaise, and butter are the examples of emulsions. For example, butter has a continuous lipid phase surrounds water droplets, so water-in-oil emulsions are formed. On the other hand, milk is an example of the oil-in-water emulsions.

Emulsions can be unstable, because free energy is associated with the interface between the two phases. As more and more emulsions are formed, the interfacial area increases, therefore, more energy is required to keep the emulsions from coalescence. For example, by mixing oil and vinegar salad dressing, unstable emulsions will be formed; in addition, they will aggregate together and small droplets will combine to form larger size droplets if we do not shake it continuously. In order to prevent coalescence, surfactant or emulsifier can be used. For our system, sodium dodecyl sulfate (SDS) is used which serves as a surfactant to stabilize the interface between the two immiscible liquids. Moreover, detergent is another surfactant that will chemically interact with both oil and water, thus stabilizing the interface between oil and water droplets. Besides coalescence, creaming is another property of emulsions. Creaming is the migration of one of the liquids to the top of the emulsion under the influence of buoyancy or gravitational force.

Monodispersity of emulsions is an important factor that people consider in colloidal science, because a wide size distribution would prevent the crystalline phases formation

1.2. ELECTROSPRAY

A sufficiently high electric field applied to the surface of a liquid causes the emission of fine charged droplets. This spraying process was discovered many years ago. In ambient air, it is generally observed by applying a potential difference of several thousand volts between a plate and the end of a capillary supplied with liquid. This type of spraying has been investigated by many authors in connection with various applications, such as: surface coatings, agricultural treatments, emulsion or aerosol production, fuel spraying, micro encapsulation, ink-jet printers and energy conversion. In vacuum the electric field is not limited by the appearance of corona discharges and the velocity of the particles is not limited by aerodynamic drag. It is then possible to atomize liquids having a very high surface tension, to obtain electric currents higher than in air and to produce extremely fine droplets or even atomic or polyatomic ions[76]. This has led to research in such areas as electrical propulsion in space, microlithography and different uses of ion beams or metallic micro droplets.[56]

All these investigations[70] have demonstrated the complexity of electrostatic spraying phenomena; this process is still not fully controlled. Many parameters are involved, the most important of which are:

- the physical properties of the liquid, and in particular its electrical conductivity, its surface tension and its viscosity;
- the liquid flow rate;
- the applied voltage;
- the geometry of the system used;
- the dielectric strength of the ambient medium.

The following empiric formula shows how the flow rate and other properties affect the diameter of the droplet by using an electric field.

$$d^* = Q^{*2/3}[0.37 + 0.49Q^{*-0.11}\exp(-0.56Q^{*1/2}V^*)]$$

$$Q^* = \frac{\rho k Q}{\epsilon\epsilon_0\gamma} \qquad d^* = \left(\frac{\rho k^2 d^3}{(\epsilon\epsilon_0)^2\gamma}\right)^{1/3}$$

$\varepsilon_{1,0}$; electric permittivity of the liquid and the surrounding gas respectively

V; applied voltage

d; diameter of the droplet

Q; flow rate

k; electric conductivity

ρ; density

γ; surface tension

Depending on the values of these parameters, different functioning regimes or "modes" are obtained, giving aerosols of highly varied characteristics and of inequal practical value. More information is given in attachment 1.

1.2.1 CONE-JET MODE

One of the most interesting functioning modes is the one in which the meniscus takes on the form of a cone extended at its apex by a permanent jet whose breakup gives rise to the droplets (**Figure 1.**). This mode was observed for the first time by Zeleny. Vonnegut and Neubauer have doubtlessly achieved this mode during their first experiments on electrical atomization for liquids such as distilled water and alcohol. It has been investigated since by many authors and has been given various names. In the absence of a consensus, we shall use the compound word "cone-jet" which simply denotes the form taken on by the liquid at the outlet of the capillary without prejudging the manner in which this configuration is maintained.

1.2.2 CONE-JET CONFIGURATION

For liquids of relatively high conductivity, the appearance of a conical shape makes it possible to obtain a jet of very small diameter compared with the capillary diameter. Several studies were conducted to provide a theoretical justification for the existence of such menisci.

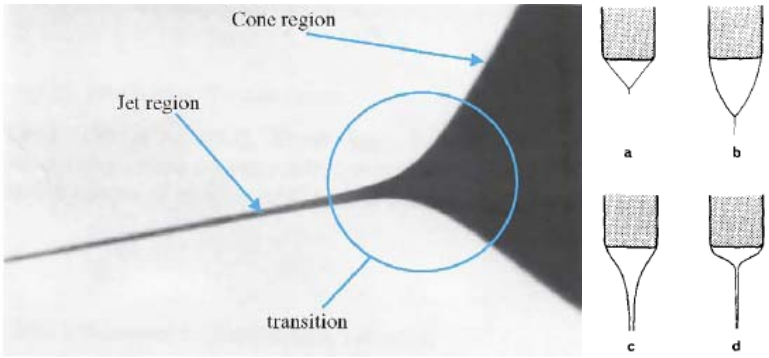

Picture taken from Jorge Carretero y Manuel Martinez Sanchez.

Figure 1. Cone Jet Mode.
a) Cone-jet mode symbols. **b)** Different forms of the meniscus in the cone-jet mode. *Reference: M. Cloupeau and B. Prunet-Foch*

1.3 PHASE TRANSITION IN DISCOTIC SYSTEM

Dispersions of colloidal particles have been observed to mimic the behavior of atoms and molecules in certain respects. Monodisperse spheres may crystallize into highly ordered structures. The arrangement and density of particles in such structures depends on the range of interactions in relation to the size of the particles. These systems have attracted considerable interest as their larger size gives rise to much slower motion than atomic or molecular materials. Dynamics of phase separation can then be followed using convenient time-scales. It is also possible to tailor systems with particular interactions or mixtures of particle sizes to explore the origin of particular behavior.

Large molecules with a plate-like or discotic form are known to form a range of thermotropic mesophases. In some cases columnar phases are observed. At

higher temperatures, or on dilution with solvent, less-ordered phases such as a nematic can be found. These systems demonstrate the fine balance in determining the phase behavior in different systems. Specific interactions generated by dipolar force and hydrogen bonding can give rise to more complex structures such as cholesteric and twisted phases.

1.3.1 PHASE BEHAVIOR OF A MIXTURE USING NON ADSORBING POLYMER

The addition of nonadsorbing polymer to a suspension of colloidal particles gives rise to a so-called depletion attraction, which originates from the overlap of the depletion zones from which the polymer expelled as the colloids approach (**Figure2.**). For separations between the particle surfaces smaller than the size of the polymer coil, the osmotic pressure of the polymer Π_p gives rise to a depletion attraction between the colloids

$$W_{\text{dep}} \simeq -\Pi_p V_{\text{ov}}$$

where V_{ov} is the volume by which the depletion zones of the colloids overlap. The colloid-polymer model that is almost exclusively studied in these model studies is that of hard-sphere colloids and polymers. The phase diagram of such mixtures has been shown to be determined by the range and the depth of the depletion attraction, which in the experiment can be tuned by the size and concentration of the polymer.

Compared to the phase behavior of spherical colloids and polymer, the phase behavior of mixtures of anisometric i.e., rod or platelike particles and polymer is even richer due to the possibility of forming liquid-crystal phases. A more comprehensive understanding of the rod polymer phase diagram has been raised by experiments on well defined colloidal model systems of rods and polymers, theory, and simulations.

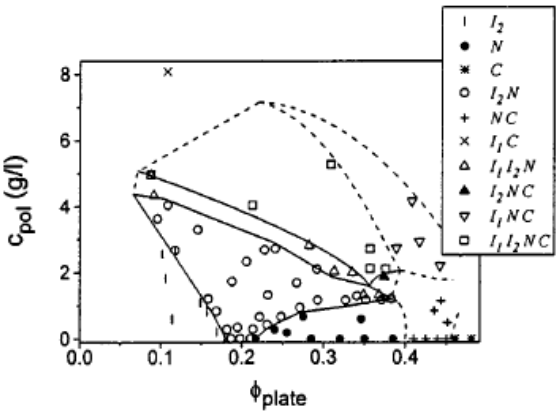

Figure taken from F. M. van der Kooij and H.N.W. Lekkerkerker.

Figure 2. The experimental phase diagram of the plate/polymer mixtures.
Phase boundaries are indicated by lines, their shape and positioning being based on the data points they enclose, and on the consistency with surrounding phase regions. Lines are dashed in cases where the location of the phase boundary is not known precisely due to local scarcity of data points.

Next to broadening of the isotropic-nematic coexistence region, depletion attraction is found to enrich the phase behavior of rods by enhancing the stability of liquid-crystal phases nematic, smectic and by introducing an additional isotropic or nematic phase.

The actual effect of the attraction depends on the range and depth of the depletion potential, as well as on the anisometry and polydispersity of the rods. Largely unexplored, however, is the phase behavior of mixtures of platelike colloids and polymer. While the phenomenon of depletion attraction does play a role in drilling fluids comprising platelike clay particles and polymer, the attraction thus raised, causes aggregation and gelation rather than equilibrium phase transitions. This behavior may actually point at an intrinsic tendency of plate-polymer mixtures to form nonequilibrium states, originating from the relatively large overlap volume of the depletion zones of parallel plates compared to that of rods or spheres.

1.3.2 LIQUID CRYSTAL PHASE TRANSITIONS IN SUSPENSIONS OF PLATE-LIKE PARTICLES

Colloidal suspensions that form periodic self-assembling structures on sub-micrometers scales are of potential technological interest. Colloidal particles with non-spherical shapes (such as rods and plates) are of particular interest because of their ability to form liquid crystals. Nematic liquid crystals possess orientational order; smectic and columnar liquid crystals additionally exhibit positional order (in one or two dimensions respectively). However, such positional ordering may be inhibited in polydisperse colloidal suspensions. Here we describe a suspension of plate-like colloids that shows isotropic and columnar phases on increasing the particle concentration.

Colloidal particles are hardly ever truly monodisperse but often exhibit a size distribution of finite width. The consequences of this inherent polydispersity are of substantial fundamental and industrial interest. In particular, the inhibite role of polydispersity in the crystallization process of hard spheres is a contentious issue that deals with the value.

Moreover, one may wonder how polydispersity affects positional ordering if such ordering exists in just one or two dimensions, that is, in the case of smectic or columnar liquid crystals. For dense system of rods, computers simulation predicts stable smectic phase up to a polydispersities the smectic phase is pre-empted by a columnar phase. Accordingly in experiments, almost monodisperse rod-like virus particles show a smectic phase while polydisperse solutions of DNA-rods show a columnar phase instead.

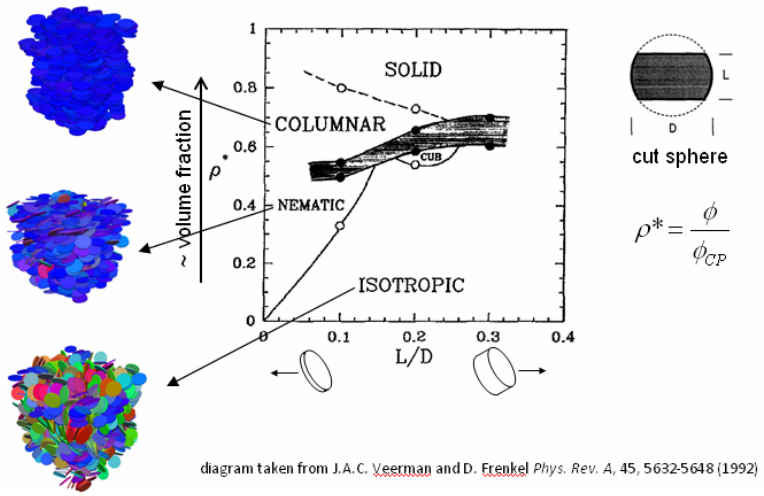

Figure 3. Phase diagram hard disks from Monte Carlo Simulation.

The phase behavior of hard plate-like particles, on the other hand, has received considerably less attention, largely because suitable experimental mode systems have been developed only recently. One of these model systems, comprising fairly monodisperse platelets of low aspect ratio, exhibits an isotropic and columnar phase; but, computer simulation done by Frenkel for monodisperse platelets of sufficiently large aspect ratio predicts an isotropic (I) a nematic (N) and a columnar (C) phase upon increasing the concentration of platelets as shown in **Figure 3**.

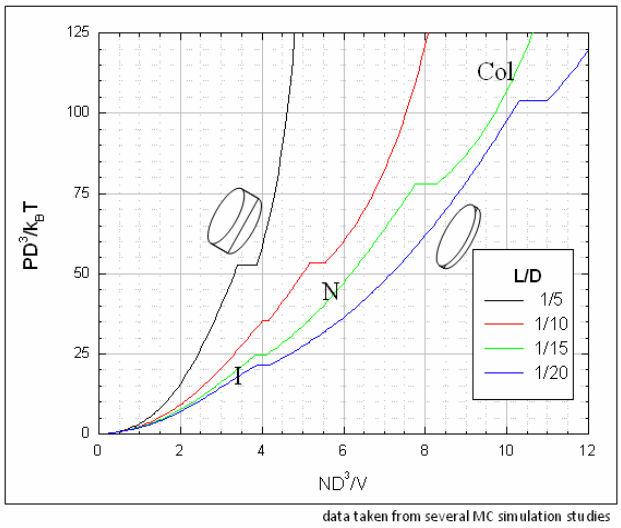

Figure taken from H.N.W. Lekkerkerker.

Figure 4. Equation of state of several aspect ratios.

The aspect ratio affects the phase transition for each particular case. The Figure shows the energy is needed vs. the concentration for different aspects ratios for emulsions of plate-like particles.

Unlike the columnar phase, a smectic phase is not sensitive to polydispersity in diameter, as ordering within the smectic layers is liquid-like. Instead, the smectic requires a low polydispersity in thickness. The relative stability of nematic, columnar and smectic phases is therefore determined not only by the volume fraction of the suspension and the polydispersity in diameter, but also by polydispersity in thickness. Computer simulations based on thickness influence in a discotic system are shown in **Figure 4.**

1.4 LIQUID CRYSTAL MATERIALS

Liquid crystals were first discovered in 1888 by the Austrian chemist Friedrich Reinitzer when he was conducting experiments on a cholesterol based substance. He discovered that the substance has two different melting points, and later on, he named this material as “liquid crystal” since it shares both properties of solid and liquid phase. Between liquid and solid phases, liquid crystals appear in different phases when temperature changes. Isotropic phase is the one that has the property closest to liquid phase. It has the highest number of symmetry and lowest ordering of molecules, because the molecules are all randomly aligned into all different directions. **Figure 5** shows different phases of liquid crystals of rod like molecules. When temperature is lowered, kinetic energy of molecules in isotropic phase is reduced; molecules in isotropic phase will orient themselves into a certain position to maximize entropy and changes into nematic phase. Nematic phase has lower symmetry and higher degree of ordering of molecules than the isotropic phase. Molecules in the nematic phase are oriented on average along a particular direction, but they still have random translational motions. As temperature is further decreased, molecules are changed into the smectic phase. The smectic phase has even lower symmetry and higher degree of ordering than the nematic phase. Molecules in the smectic phase are aligned into layers or planes. They have

translational motions within a single layer, but not between layers. As temperature is further decreased, the smectic phase will be changed into the crystalline phase. Crystalline phase has the lowest symmetry and highest degree of ordering, because molecules are regularly ordered in position and aligned in only one direction.

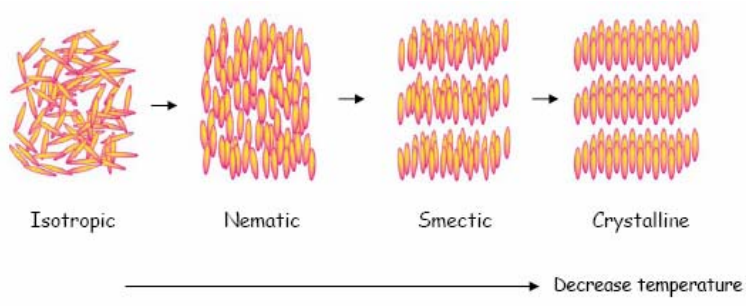

Figure taken from Sussana Wong, Dr Cheng group.

Figure 5. Different phases of liquid crystals of rod-like molecules between liquid and solid phase.
As temperature decreases, molecules change from isotropic, nematic, smectic, and finally to the crystalline phase.

Furthermore, liquid crystals made of disk shaped molecules or particles are the least studied compared to others made of such as rod shaped molecules or particles. This thesis contributes to the study of discotic liquid crystals by producing uniform wax disks using electrospray.

Similarly to the rod shape molecules, disk shaped molecules can also orient themselves into discotic isotropic, discotic nematic, and discotic columnar phases. **Figure 6** shows different phases of discotic liquid crystals. Depending on the temperature, disk concentration or pressure, discotic liquid crystals change from isotropic, nematic, then to columnar phase. For example, by decreasing the temperature, columns in discotic columnar phase will orient themselves into hexagonal or some other rectangular shapes. Researches have been shown that different tilt angles of disk shaped molecules in columnar phase liquid crystals can form different shapes of columnar phase such as hexagonal, rectangular, oblique, rectangular face-centered, and tilted columns.

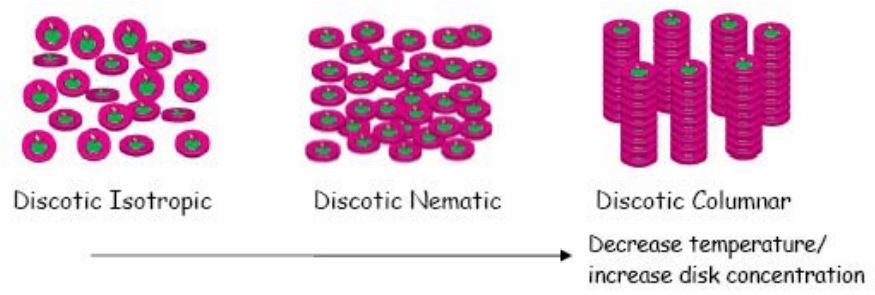

Figure taken from Sussana Wong, Dr Cheng group.

Figure 6. Different phases of discotic liquid crystals of disk-like molecules.

As temperature decreases or disk concentration increases, discotic liquid crystals change from isotropic, nematic, then to columnar phase.

1.5 THE EFFECTS OF SURFACTANTS IN EMULSIONS

Sodium dodecyl sulfate (SDS) [CH_3-$(CH_2)_{11}$-OSO_3^--Na^+] is an amphiphilic molecule which consists of a hydrophilic polar head and a hydrophobic non-polar tail. At high concentrations of SDS, SDS monomers aggregate into structure called micelles. A micelle is thermodynamically stable aggregation, where the non-polar tails are sequestered inward to avoid exposure to water, and the polar heads are oriented outward in contact with aqueous solution. This configuration avoids the contact of the hydrophobic tail with water, and minimizes the energy. The **Figure 7** shows the SDS monomer; and SDS monomers formed micelle. SDS is used to stabilize the interface between two immiscible liquids. In this experiment we use α-eicosene dissolved ethanol and diluted SDS in deionized water.

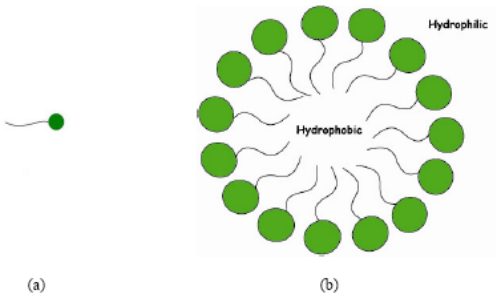

Figure taken from Sussana Wong, Dr Cheng group.

Figure 7. Emulsification with surfactants.

(a) Sodium dodecyl sulfate (SDS) monomer consists of a hydrophilic polar head and a hydrophobic non-polar tail. **(b)** SDS micelle formed by hydrophilic polar heads orienting outward in contact with water, and hydrophobic non-polar tails sequestering inward to avoid exposure to water.

1.6 BIREFRINGE OF LIQUID CRYSTALS.

Birefringence is one of the salient characteristics of liquid crystals, and it occurs in anisotropic phases: nematic, smectic, and crystalline phases. Liquid crystals experience birefringence due to the orientation characters, alignments and shapes of their molecules. Optical axis is the straight line passes through the centers of curvature of the lens surfaces, and when light travels along this axis would not be deflected in any direction. The electric field is everywhere perpendicular to the optical axis, and it is called the ordinary (o-) ray. Ordinary ray travels at the same velocity in every direction through the anisotropic materials. The light wave with the electric field parallel to the optic axis is called the extraordinary (e-) ray. Extraordinary ray travels at a velocity that depends on the propagation direction within the anisotropic materials. Birefringence defines as the difference in refractive indices, $\Delta n = n_e - n_o$, between the ordinary (n_o) and extraordinary (n_e) rays. The retardation between the ordinary and extraordinary ray increases with increasing the anisotropic material's thickness.

Because of the birefringence of the disks, they are observed under the polarized light microscope as shown in the following figures.

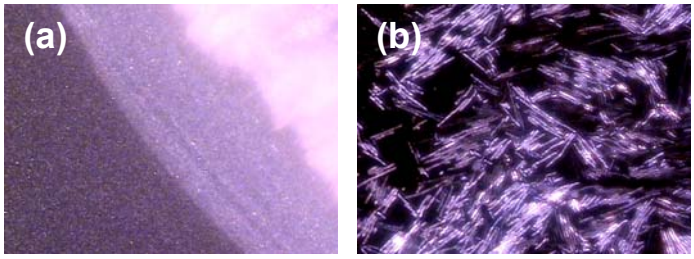

Pictures taken from the author.

Figure 8. Birefringent disks under cross polarizer microscope.

(a) Wax particles were formed using α-Eicosene. **(b)** Birefringent micro-disks were formed by keeping the temperature lower than 4ºC due wax properties**.** The micrograph was taken using a polarized light microscopy. Diameter of the α-eicosene disks on average is about 4 μm.

2. EXPERIMENTAL SECTION

2.1 ELECTROSPRAY EMULSIFICATION

The wax of α-Eicosene (Sigma-Aldrich Corp. St Louis MO) was used as received, with 1% (w/w) of STADIS-450[70] (Octel Starreon, Newark, DE) added to increase its electrical conductivity. A mixture of 200mL of ethanol and water (80/20 w/w) was prepared, to which 0.005 wt% of Tergitol 15-S-9 (Sigma-Aldrich) and SDS of 20 mM was added[68]. This mixture was used to collect the wax droplets in a 500mL beaker, as illustrated in **Figure 9a**. An electric heater was employed to maintain local environment temperature of α-Eicosene higher than its melting point (26°C).

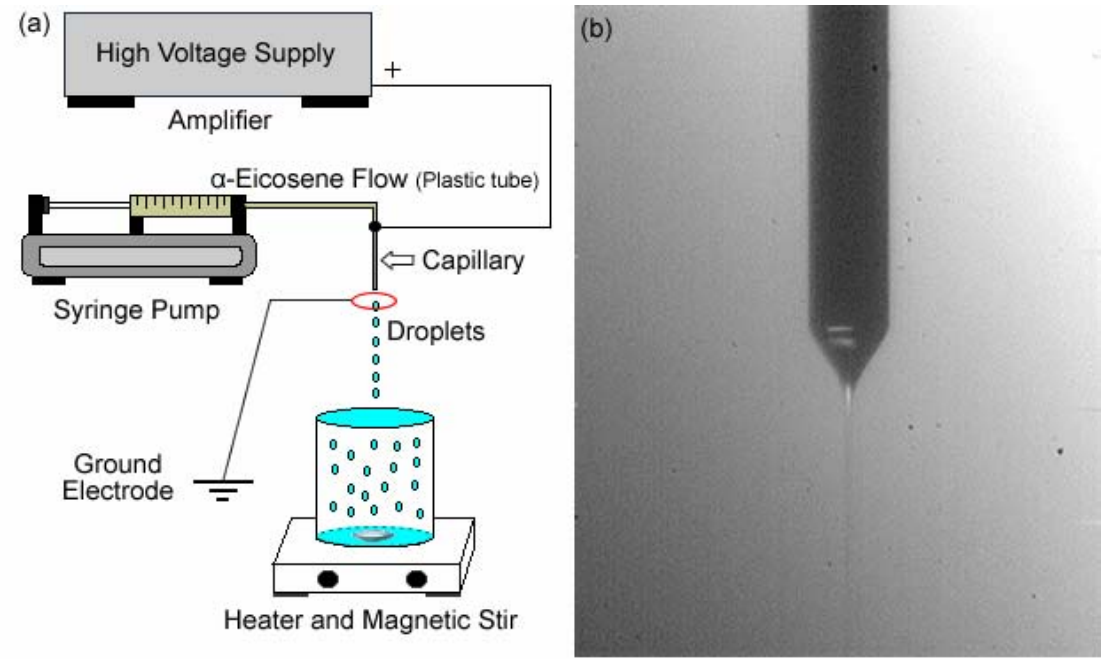

Pictures taken from the author.

Figure 9. Electrospray emulsification setup.
(a) Schematic setup. A strong electric field was generated between a capillary needle and a ground wire-ring. The collection solution was heated to tune the density and surface tension, and stirred to facilitate drop entrance. **(b)** Micrograph showing a stable cone-jet mode of electrospray.

Liquid wax was introduced through a metallic needle using a syringe pump. A digital signal generator and a high voltage amplifier were used to provide the required high electric voltage. The positive electrode was connected to the top side of the needle, beneath which there was a grounded circular wire. The distance between the tip of the needle and the surface of the SDS solution was kept at 7 cm. The solution was heated to adjust the density and surface tension of the collection fluids. A magnetic stir was used to homogenize the resulted emulsions. A stable Taylor cone was observed (**Fig. 9b**) with a voltage range from 2.6 to 2.9 kV, we observed. For α-Eicosene flow rate ranging from 1 ml/hr to 10 ml/hr, the jetting liquid from the cone broke into fine droplets with a fairly narrow size distribution. Ethanol was added to the collection solution to match the density of wax, and was later evaporated at room temperature because ethanol slightly dissolves α-Eicosene. Before the evaporation of ethanol, another 160 mL of water was added to prevent aggregation arise from increase of SDS concentration after evaporation (which introduces depletion attraction between wax droplets). By controlling the surfactant concentration, we were able to obtain metastable emulsion.

2.2 ANALYSIS OF CREATING EMULSIONS USING ELECTROSPRAY

In electrospray, the droplet size is dominantly controlled by the liquid flow rate and secondarily by the applied voltage, but independent of the capillary size[70]. For a given liquid, the Taylor cone can only be established in a certain range of liquid flow rates and voltages, which depend on the electric conductivity of the liquid. As conductivity increases, the range shifts toward smaller flow rates, and smaller droplets were generated in the spray[70]. The electric conductivity of wax is linearly dependent on the added Stadis 450 concentration. In our experiments, the desired conductivity (4.1×10^{-8} 1/Ω cm) was achieved by adding 1 wt% of Stadis 450 to α-Eicosene. For the given experimental conditions, it was found that the size of the droplet has no dependence on the amount of added additive.

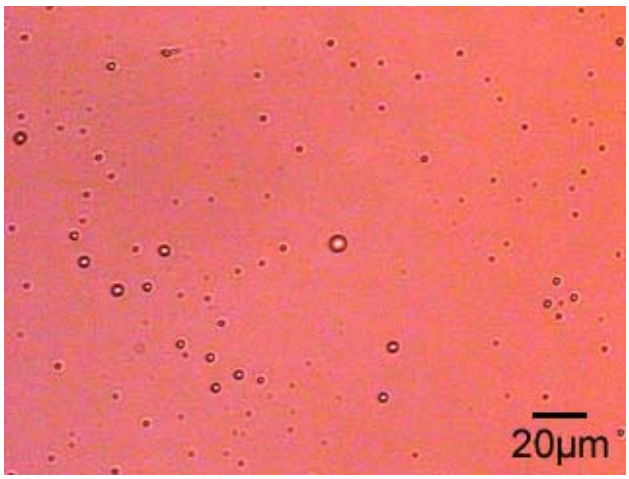

Picture taken from the author.

Figure 10. Polydispersity in electrospray.

Size polydispersity was evident when wax droplets were collected in solution with mis-matched density and surface tension. The collection fluid is 20mM SDS aqueous solution. The flow rate is 4ml/h and the applied voltage is 2.8 kV.

We measured the size distributions of the wax droplets using an optic microscopy (Nikon TE2000-U) after the emulsion was cooled down to room temperature. **Fig. 10** shows the particles collected using pure water, with no ethanol added. The polydispersity in size was evident. Water mismatches the density and surface of α-Eicosene. The density mis-match is a serious issue in emulsion formation process where the drop entrancement is of vital importance. As a result of density mismatch, the wax droplets tend to spread on the water-air interface. Later, when particles raised to the water-air interface due to buoyancy force, they would coalesce with the incoming newly produced droplets from electrospray. This could be evidenced from the chunky pieces of wax were found on the air-water interface.

When using ethanol-water mixed solution, Tergitol as surfactant, and by optimizing temperatures, we were able to reduce the mis-match in density and surface tension. The droplets enter the solution immediately after they touch the solution surface.[89] We found that the surface aggregation of the droplets was

prevented using 20-80 w/w water/ethanol solution with density close to that of α-Eicosene. At 40°C the density of water is 0.992 [kg/m^3], ethanol is 0.773 [kg/m^3], α-Eicosene 0.795 [kg/m^3], and 20-80 w/w water/ethanol is 0.817 [kg/m^3][90]. We added Tergitol 15-S-9, a nonionic secondary ethoxylated alcohol to the collection liquid which can control surface tension effectively[91].

Drop entrancement is complicated due to the finite difference in interfacial tension between air-water and air-wax droplets. Experiment by Li and Wang[89] has showed that the falling drops of wax often spread on the surface rather than entering the water, due the hydrophobic nature of wax and hence a positive spreading coefficient S as defined in the following equation.

$$S = 2\sqrt{\sigma_p}(\sqrt{\sigma_c} - \sqrt{\sigma_p}).$$

Where $\sigma_c = 23.5\times10^{-3} N/m$ is the surface tension ethanol/water solution[90] at 80/20 and $\sigma_p = 29\times10^{-3} N/m$ is the α-Eicosene surface tension[92], both valued at 40°C. When the surface tension of water is larger than the wax droplet, the spreading coefficient is positive causing the drop to spread out. The spreading coefficient must be made negative in order to allow the droplets enter the water intact by reducing the surface tension of water using ethanol or surfactants.

Figure 11 shows the images of wax droplets collected using 80/20 w/w ethanol/water. The spherical wax droplets are 4.07±0.02 μm in diameter. The polydispersity is less than 5%. Ordered lattice structure is observable confirming the narrow size distribution of the droplets. The same microscope was used as in **Figure 10**.

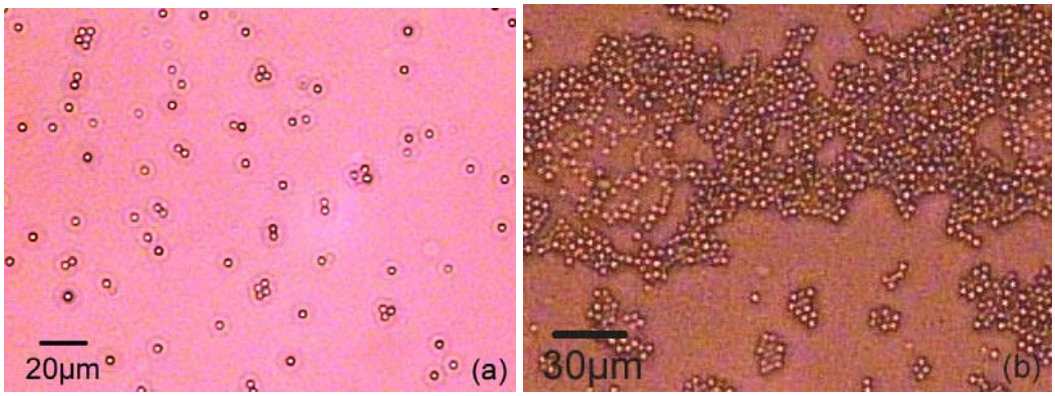

Picture taken from the author.

Figure 11. Monodisperse suspensions in electrospray.

A monodisperse suspension produced with a collection solution of 80%w ethanol, 20%w water and 20mM SDS. The flow rate is 4ml/h and voltage 2.8kV. **(a)** Micrograph of 20x magnification **(b)** 10x.

The sample was kept at low temperature (4^{o}C), and checked frequently for the morphological changes of wax particles using polarizing optical microscopy.

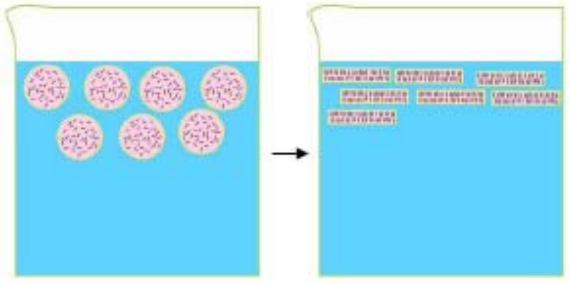

Figure taken from Sussana Wong, Dr Cheng group.

Figure 12. Generation of disk particles.

Generation of disk-like particles through isotropic-smectic phase transition.

As particles creamed, columnar phase was observed at high concentration as shown in **Fig. 13**. Microdisks stake into columns, and columns intend to bundle. The straight columnar morphology demonstrated the narrow size distribution of the microdisks that are transformed from the monodisperse wax droplets. The structure of the columar phase is similar to the stacking of red blood cells in the rouleaux. [93, 94]

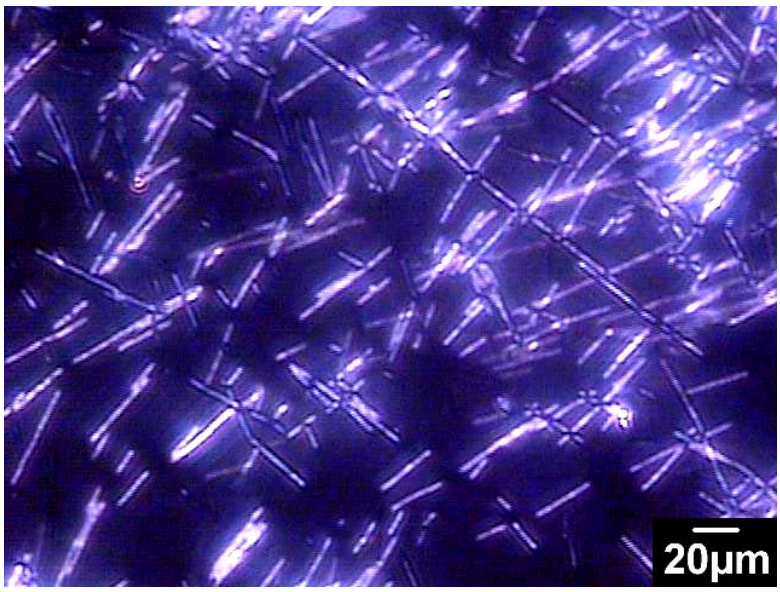

Picture taken from the author.

Figure 13. Columnar phase in wax disks.
Columnar phase observed at high disk concentration.

We are able to mass-produce microdisk supensions[68] at the rate of a few mili-liters per hour. This new emulsification method is a nature extension to the microfluidic emulsification to produce monodispersed emulsion droplets of tens of microns[95, 96]. It open doors to further characterization of discotic colloids, one of the least studied types of colloids[39, 43, 46, 48].

3. SHAPE CHANGES EMULSION

We made uniform wax emulsions by electrospray of melted α-eicosene at 60^{o}C and collected in 10 mM SDS aqueous solution. After keeping at 4 ^{o}C for two weeks, the wax particles exhibit an optical morphology resembling the red blood cells. **Figure 14a.** Presents single disks. **Figure 14b.** Shows rods assemble of these wax platelets.

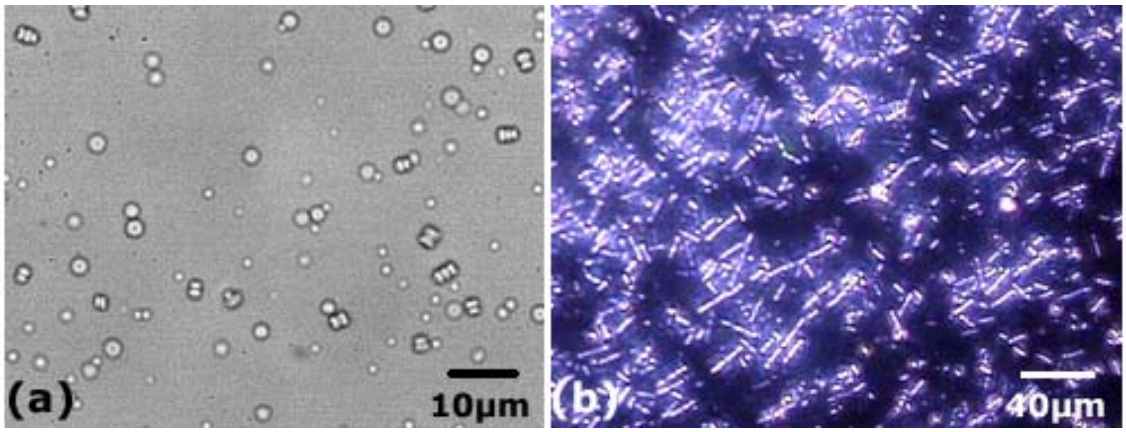

Pictures taken from the author.

Figure 14. Pictures of the colloids particles looking like red blood cells.

(a) Magnification using 100x lens of the red blood cells disks showing their defects with an aspect ratio of **L/D = (1/2).** The disks show a rouleaux formation in a high concentration solution in some cases resembling the interaction of the real red blood cells. **(b)** Assembly of the disks like red blood cells. Inverse light polarizer was used.

According to the Langmuir isotherm of SDS adsorption to self-assembled monolayers (SAMs) with neutral electric charge[97], the surface excess of SDS at the water-SAM interface Γ as a function of SDS c concentration is,

$$\Gamma = \frac{\Gamma_m k_L c}{1 + k_L c}$$

With the maximum adsorption density $\Gamma_m = 1.1 \text{ molecules} / nm^2$ and the Langmuir equilibrium adsorption constant $k_L = 180 M^{-1}$. Assuming the adsorption of SDS to α-eicosene surface be similar to this SDS-SAM isotherm, we estimate the surface

adsorption density of SDS is about $\Gamma_{10mM} = 0.71 \text{molecules} / nm^2$ with 10mM SDS aqueous, which is about 27% of the density of dehydrated SDS crystalline packing. Our experiment indicated that 27% mixing of SDS into α-eicosene is not high enough to make flat disk surface. The dimple in the center of the particles might due to the partial phase separation between α-eicosene and SDS molecules.

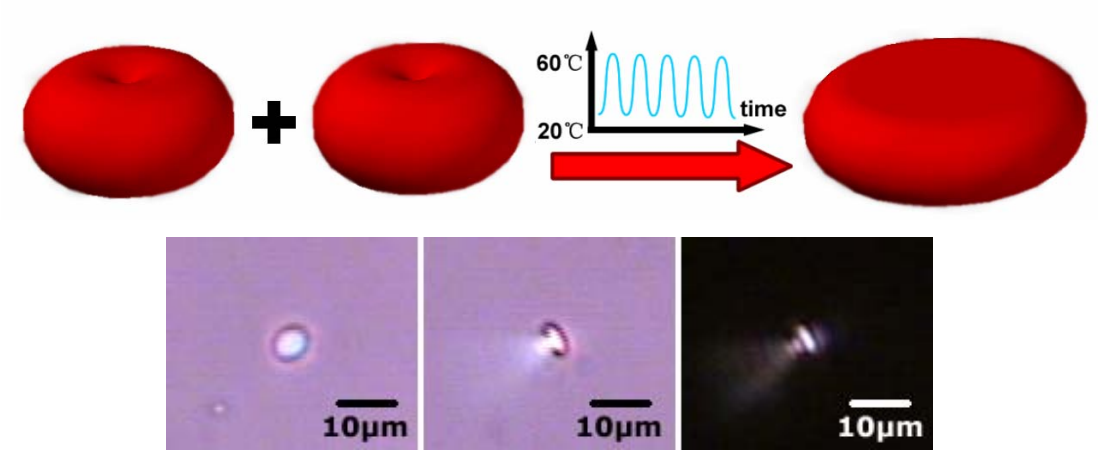

Pictures taken from the author.

Figure 15. Coin like disks hypothesis.

The coalescence between two disks like "red" blood cells increasing the surface SDS concentration. The disks are attracted to each other due the high sample SDS concentration. Temperature was raised and lowered for several times between 20 and 60 oC. The high temperature was over the melting point of the α-Eicosene. This procedure produced disks of larger volume and a larger aspect ratio **L/D = (1/4).**

We increased the SDS concentration to 60 mM to introduce stronger depletion between the spherical wax emulsions[68, 98], and rise and cool the suspension several times to cause coalescence of the dimmer aggregates (**Figure 15**). The surface area decrease by 1.26 times when two spherical droplets coalescence into one bigger one. So the SDS surface density become 0.89 molecules/nm^2, cover the interface about 35%. We observed two flat circular surfaces for these large particles. Let assume that there is not phase separation between eicosene and SDS when the surface overage is larger than 33%. From the observed dimple size 10% of the diameter, we estimated that the dilute phase located at the dimple has

about 5% SDS. The kinetic for the shape change measured by the appearance of birefringence is one order of magnitude faster for the one with 35% SDS coverage (1 day) than the 27% coverage (2 weeks). We consider that 35% surface coverage of SDS is just above the threshold to induce surface crystallization at the α-eicosene-water interface, and the layering propagated into the isotropic phase to make rotator phase.

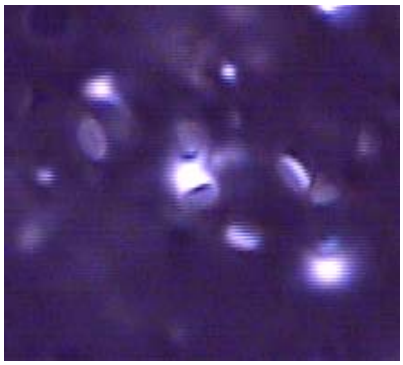

Picture taken from the author.

Figure 16. Coin like disks system.

Disks fabricated using 10:1 decanol:SDS in a 10mM SDS aqueous solution. The co-surfactant decanol could achieve a high surface concentration and form a condensed phase at the wax-water interface, which induce surface freezing of the wax. The wax microdisks are uniform in volume and aspect ratio **L/D = (1/4).**

As long as we realized that higher surface concentration of surfactants is required to fabricate flat disks, we use a co-surfactant, decanol, to tune the organization of molecules at the interface. Decanol is expected to increase the surfactant molecular packing density at the wax-water interface and lowering the curvature of the surfactant monolayer[4, 99, 100]. Previous experiment demonstrated fundamental difference in the phase behavior of the adsorption of SDS and n-dodecanol with n-dodecanol forms condensed phase while SDS exist only in a fluid-like state[101, 102]. Increasing n-dodecanol concentration, its homogeneous condensed phase forms and replace completely SDS[103]. Assuming decanol behavior similarly, we use its dense packing phase to interpret

our observation. When using 10:1 SDS:decanol in 10mM SDS aqueous solution, without the coalescening procedure, flat-surfaced short cylindroids are quickly formed from the wax emulsions in less than 12 hours. The optical micrograph is shown in **Figure 16**. This shape transition is consistent with an increased surfactant packing density at the wax-water interface, otherwise disks with a dimple will formed as shown in **Figure 14**. The rapid emergence of birefringence is again due to the surface freezing induced by the condensed phase of decanol. This is the first evidence of surface freezing at an alkene-water interface using a technique other than ellipsometry and surface tensiometry[14].

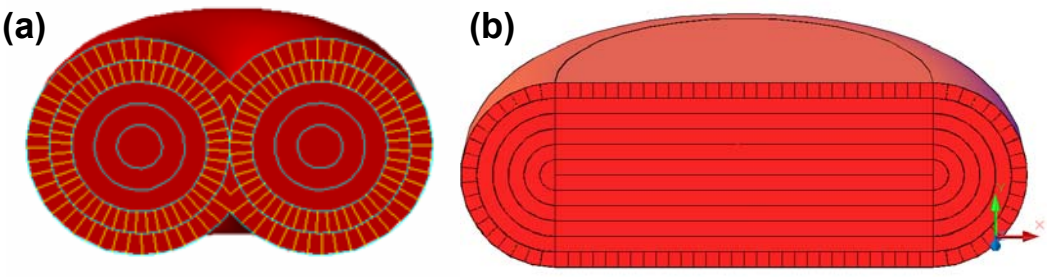

Pictures taken from the author.

Figure 17. Geometric model of both discotic systems.

Geometric model of the macroscopic defects proposed by the author. The singular lines consist of a straight line (along the axis of revolution) and a circle sitting on the isotropic SmA interface. The aspect ratio is totally different between both disks. a) RBC disk. Disk created using SDS only. b) Coin disk. Disk created using decanol as co-surfactant and SDS as surfactant

Using the stability condition for focal conics, we construct defect configuration (**Figure 17a**) of wedge, non-parallel plates, funnel domains, etc. The stability condition establishes that the layers must be equidistant on both sides of the effect interface. One relevant fact in the study of the Smectic A solutions is that any energy minimizing configuration in two dimensions must have the shape of circles or lines. The **Figure 17b** shows a coin like disks with no defects.

4. SELF-ASSEMBLY OF MICRODISKS

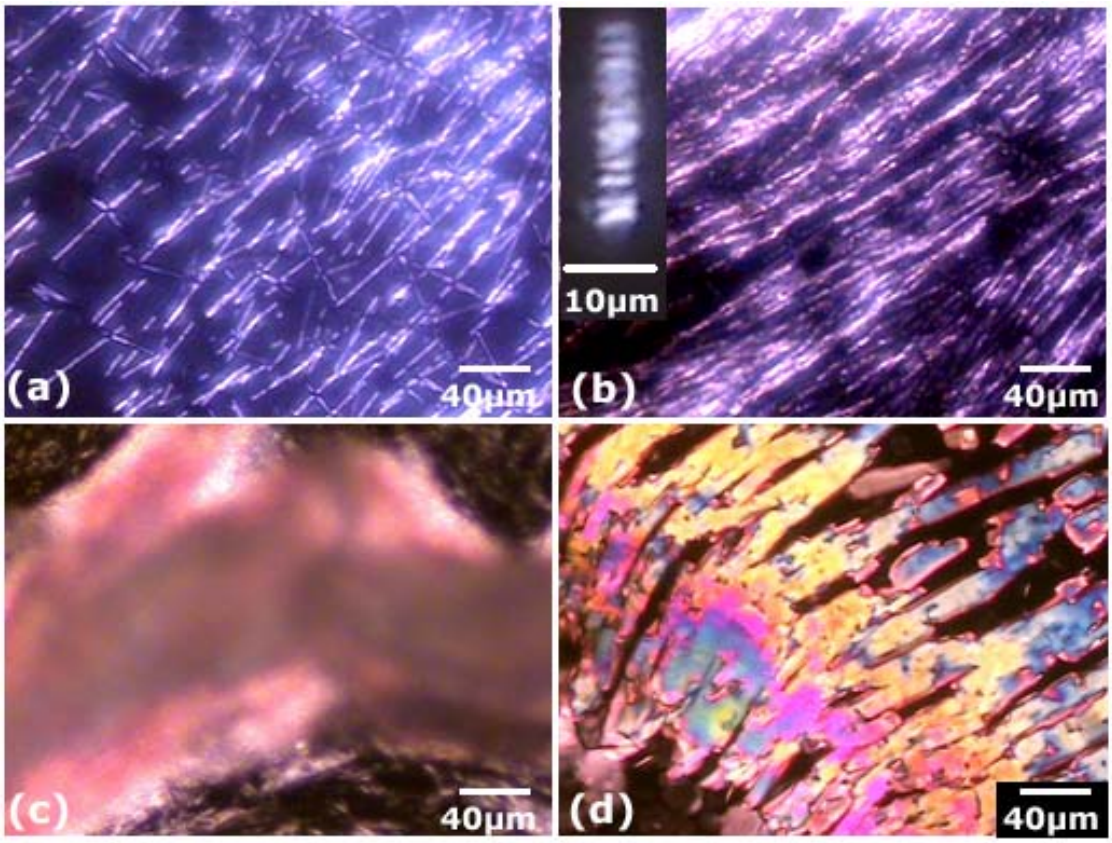

Pictures taken from the author.

Figure 18. Self assembling of micro wax disks.
Self-assembling of micro wax disks covered with decanol, observed under cross polarizing microscopy. **(a)** Low concentration suspension assembled columns longer than the disks covered with SDS only. **(b)** The columns are aligned and bundled together due to flow caused by the ethanol evaporation. **(c)** Colloidal crystals formed when columns further packing together. **(d)** Colorful domains of α-Eicosene shown after the evaporation of ethanol and water.

Depletion attraction force assembly the disks into columnar phases. **Figure 18** shows the relatively long columns form in the flat wax disks and the relatively short and “disordered” columns formed in the dimpled platelets shown in **Figure 14.**

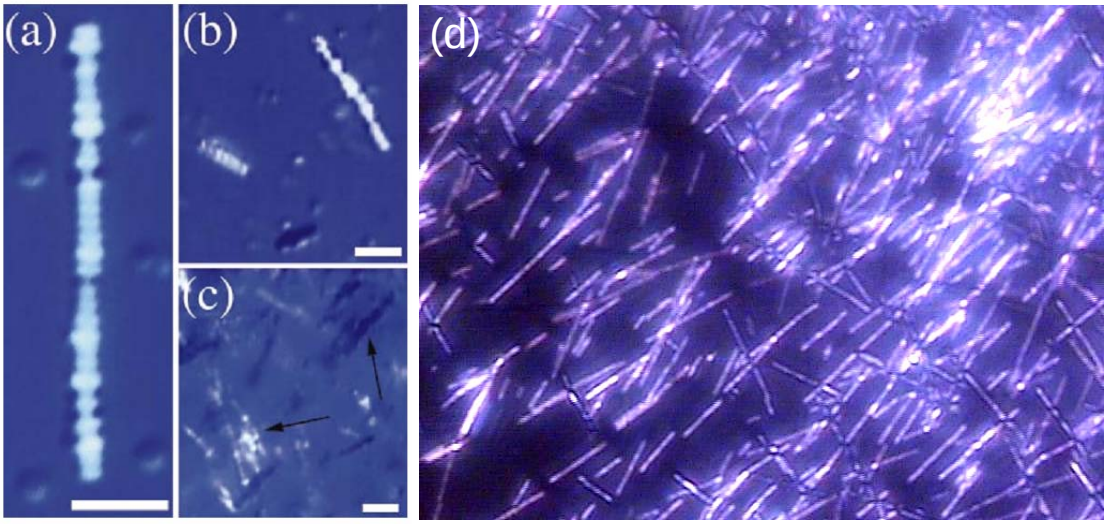

Pictures (a,b,c) taken from Mason, T. G., *Phys Rev E* 2002, 66,060402/1

Picture (d) taken from the author.

Figure 19. Mason rods vs Micro wax disks created using decanol and SDS.

Optical micrographs of **(a,b,c)** a rodlike columnar aggregate of 1-eicosene colloidal disks and unaggregated spheres in aqueous micellar SDS solution at an SDS concentration C=20mM. Scale bars are 3µm **(d)** an special improvement of the aspect ratio for the colloidal disk let to form bigger rods than other authors.

Although the columnar aggregates of disks resemble the stacked coin structures of the real red blood cells (RBCs), known as rouleaux, which form when polymers are added to blood, and the RBCs disks created by the author of the thesis, there are important differences between the two systems. Since normal and artificial RBCs have dimpled faces and, for the purpose of calculating face-face depletion interactions, resemble toroids, we would expect the largest excluded volume to resemble an annular disk. A significantly smaller concentration of micelles is sufficient to induce the aggregation of disks into columns as compared to similarly-sized RBCs

The aspect ratio has a big influence in the particles aggregation of the two different discotic systems, $\zeta = L/2R_d$, using the equation deducted by Mason before, the energy is the product of the excluded volume of micelles between the

disks and is estimated by the product of the disk facial area with the micelle diameter.

$$U^{d}{}_{c} = -2\pi R_m R_d{}^{2} \prod_m$$

The micellar osmotic pressure, $\prod_m = C_m N_0 k_B T$, where k_B is the Boltzmann's constant, N_0 is the Avogadro's number, C_m is the micelle molar concentration.

The contact energy changes with the variation of the aspect ratio. For the red blood cells the aspect ratio is (1/2) and for the coin-like disks is (1/4).

$$R_d{}^{3} = (V / \pi\zeta)$$

$$R_d{}^{2} = \varepsilon(1/\zeta)^{2/3}, \text{ where } \varepsilon = (V/\pi)^{2/3}$$

$$U^{d}{}_{c} = -\lambda_c \varepsilon(1/\zeta)^{2/3}, \text{ where } \lambda_c = -2\pi R_m \prod_m$$

Since $U^{d}{}_{c}$ is inversely proportional to the aspect ratio, disk facial area for the coin-like disks is larger than the red blood cells disks and consequently the depletion attraction between the first ones is higher than the second ones.

Increasing the disk concentration, the flat disks form colloidal crystals[104]. As the crystal and surfactants are incorporated into the disks, the smectic liquid crystal phase formed, as evident from the colorful domains in the polarized microscopy (**Figure 18d**).

5. LIQUID CRYSTAL OF EICOSENE

The **Figure 20** show us the clouds of disks melting after the evaporation of the water/ethanol drop system. As shown in **Figure 18**, many phase transitions were found, such as the Isotropic, Columnar, ¿Cubic?, but at the end of the whole process, a colorful domain took present when the evaporation finishes. We could conclude that carbon layers which were forming every individual disks were totally aligned and once the disk get destroyed –because they are not stable if no water suspension is available-, we could see those uniform colors.

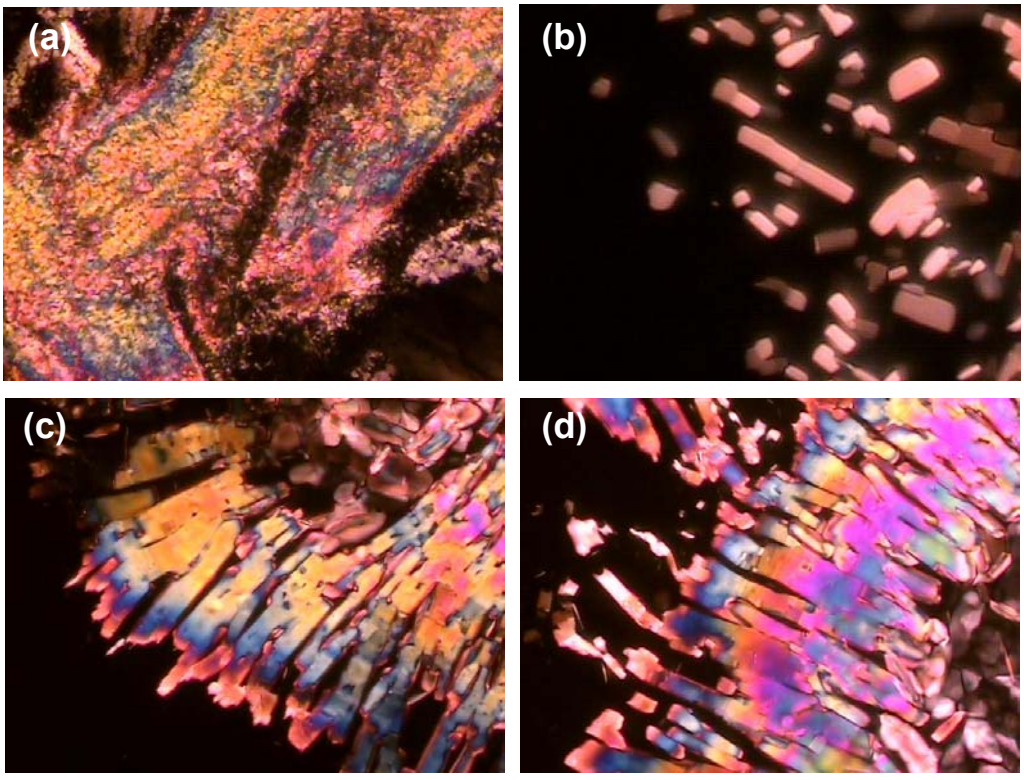

Pictures taken from the author.

Figure 20. Liquid crystal in Eicosene.

Colorful domains due the evaporation of a solution droplet which induced the self-assembling of the micro wax disks. **(a)** General view of the droplet. 50x lens **(b)** Some special and frequently shapes like bricks were found. **(c)** and **(d)** Different color domains found during the evaporation. 20x lens. Inverse polarized light was used for the pictures.

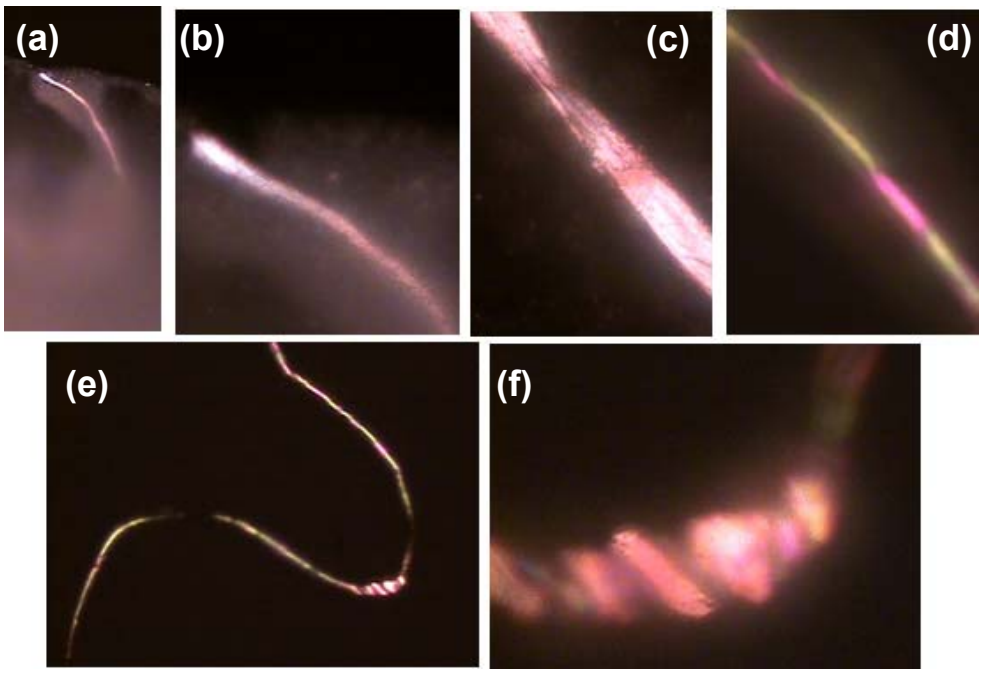

Pictures taken from the author.

Figure 21. Helical crystal formation of Eicosene.

Possible crystal was formed during the evaporation of a solution droplet. **(a)** In a full concentrated drop the disks started to aggregate like a chain. Time= 10 minutes. **(b)** A closer picture was taken of (a). **(c)** While the drop was drying and the disks were concentrating higher a helical structure started to appear. Time= 3 hours. **(d)** Completely dried drop, the chain took several and uniform colors., specially green and pink. Time = 1 day **(e)** A general view of the final helical chain. **(f)** Interesting picture of the colorful domain in a section of the chain.

Inverse polarized light was used for the pictures.

The **Figure 21** possibly presents the SmC* phase, which is one of the liquid crystal phases that can – and will – express molecular chilarity through a helical super structure. The helix axis is along the structure and the variable being helically modulated is the angle of the particles.

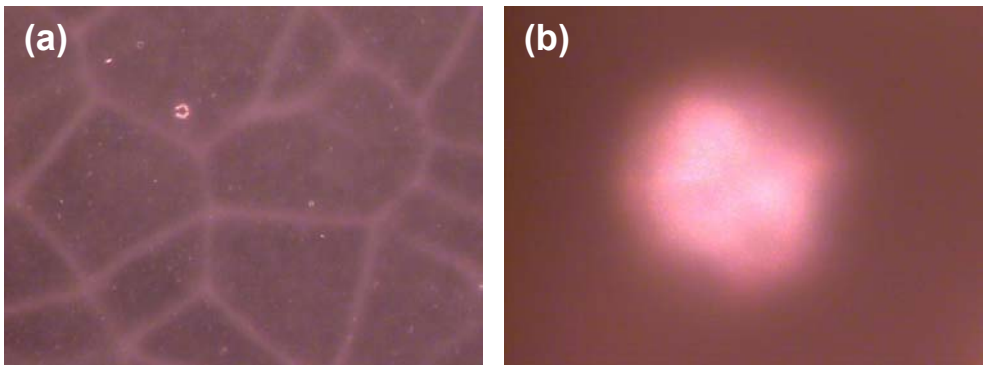

Pictures taken from the author.

Figure 22. Temporal crystal formation in a chamber.

A Chamber was filled with a full concentrated solution of disks. **(a)** The disks started to aligned in lines and small points of disks were visible. **(b)** A magnification of a random point showed us the aggregation of disks and possible formation of crystals.

Following with the experiments, a chamber was totally filled with our discotic system solution after concentrating them, in evaporation absence and no liquid evaporation motion influence, the disks started to attract each other in lines (**Figure 22a**). In the other hand, some disks created a cloud of them, presumably they were trying to organize themselves and create temporal crystals, which need lot of time to create. (**Figure 22b**).

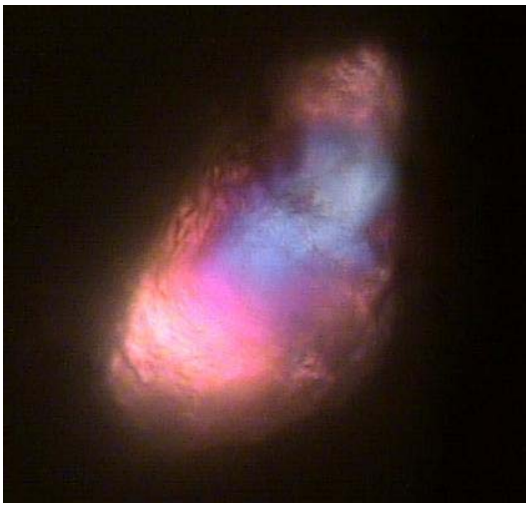

Picture taken from the author.

Figure 23. Crystal created in a chamber.

Possible crystal made with the α-Eicosene disks was made in a chamber full concentrated of disks. It took 1 week to create itself.

A week later we checked the chamber again and we found a beautiful crystal only possibly watched by polarized light microscope. We cannot assure the possible crystal formation of **Figure 22** is the same as **Figure 23**, but we can assume that those possible crystals are being formed in that way.

6. CHARACTERIZATION OF COLLOIDAL DISCOTIC PARTICLES SEDIMENTATION IN A CENTRIFUGAL FIELD

We would like to present results gained for our discotic system of colloids by using LumiSizer instrument (LUMiFuge, LUM GmbH, Berlin-Germany), which is an instrument ideally suited for characterization and optimization of dispersion properties. It quantifies particle- particle-interactions, the compressibility of particles, flocs, gels and the elastic behavior of sediments.

The packing density as function of the applied pressure was measured with the analytical centrifuge. Particle migration due to centrifugal force results in a variation of the local particle concentration and correspondingly in an alternation of the transmission. The progression of the transmission profiles contains the information on stability and kinetic of separation processes as well as on the alteration of packing density.

The job of the centrifugation machine is to increase the gravity by 2300g times into the system, in that way the whole sedimentation will not take days, just minutes to complete the process. In this case we creamed the emulsion, because α-Eicosene's density is lower than water, so the disks creamed to the top and the water was sent to the bottom of the cuvette.

6.1 THE RED BLOOD CELL DISCOTIC SYSTEM

The **Figure 24** shows the sedimentation of the red blood cell discotic system, which showed us a high attraction between the disks but it happened in a short period of time. We could make some analogies based on our pictures taken during the evaporation of the water/ethanol drop red blood cell disks system:

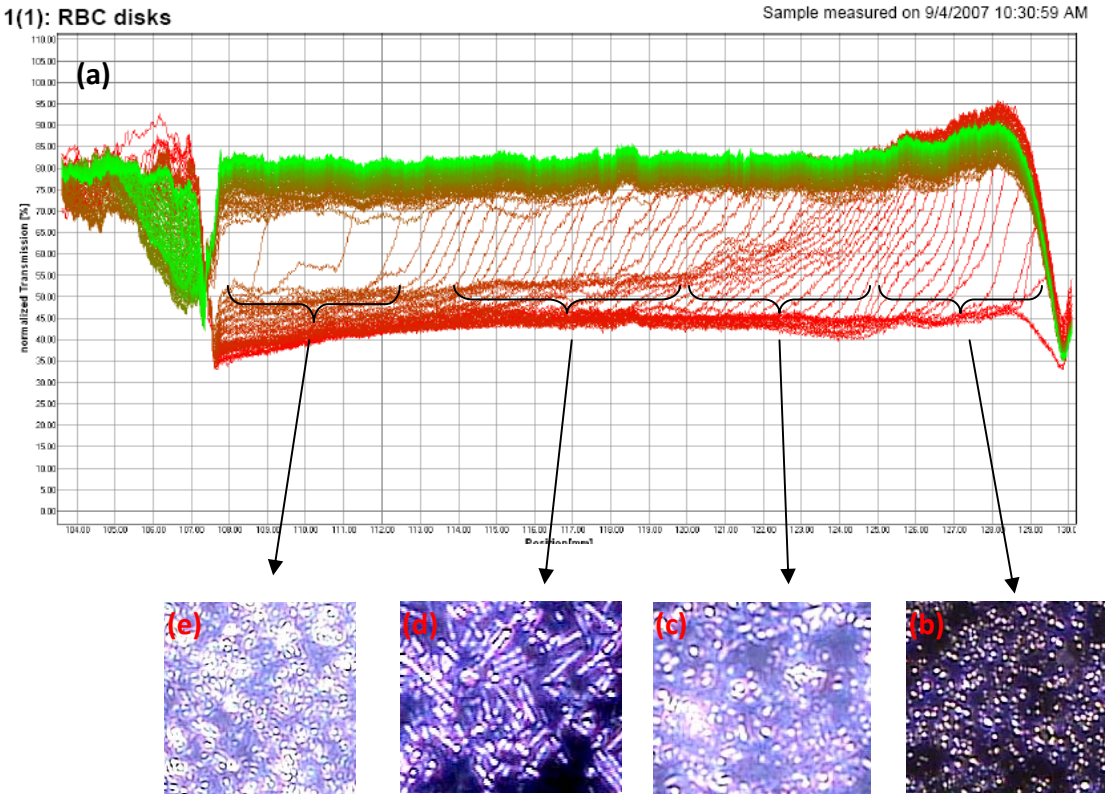

Picture taken from the author.

Figure 24. RBCs discotic system creaming in an analytical centrifugation machine.

The Figure shows the depletion attraction by increasing the disks concentration in the cuvette due the analytical centrifugation. **(a)** Transmission profile during the centrifugation. **(b)** Isotropic phase. **(c)** Cloud of disks. **(d)** Columnar phase. **(e)** The disks are starting to dry, possible crystals are forming but no color is present.

The RBCs disks system had four phase transitions, the first one was the Isotropic phase, the second was a transition phase between the Isotropic and the Columnar

phase, the third one was the Columnar phase and finally the last one was just a high concentration of disks packing together but no uniform structure was present.

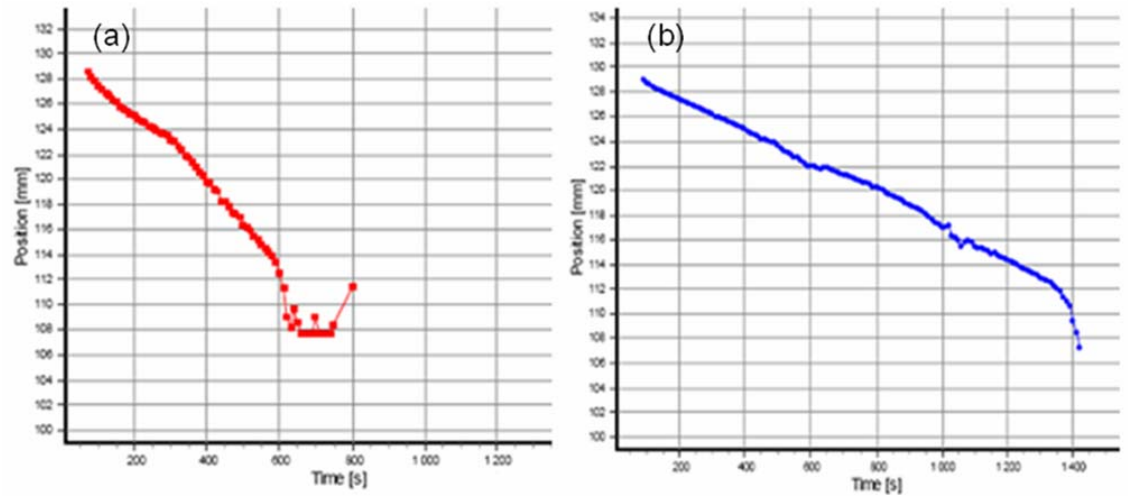

Picture taken from the author.

Figure 25. Time vs Position of RBCs discotic system.

(a) The figure shows the time it takes for the disks like red blood cells to concentrate them all to the top of the cuvette. **(b)** Time it takes the coin-like disks system to concentrate them all. The speed during the sedimentation fluctuates during the phase transition of Isotropic-Columnar and Columnar – Self organization of rods.

Figure 25 shows the Position vs. time of the creaming during the analytical centrifugation. With this data some speed data can be found during each phase, it is important for future correlations for the red blood cell and the coin like disks system.

6.2 THE COIN LIKE DISKS SYSTEM

The **Figure 26** shows the sedimentation of the coin like discotic system, which showed us a lower attraction between the disks compared with the first system (RBC disks), but the disks self assembled much more organized than the other ones. The same analogies were done like to the first system based on our pictures

doing the same experiment, watching the self assembling during the evaporation of the water/ethanol coin like disks system:

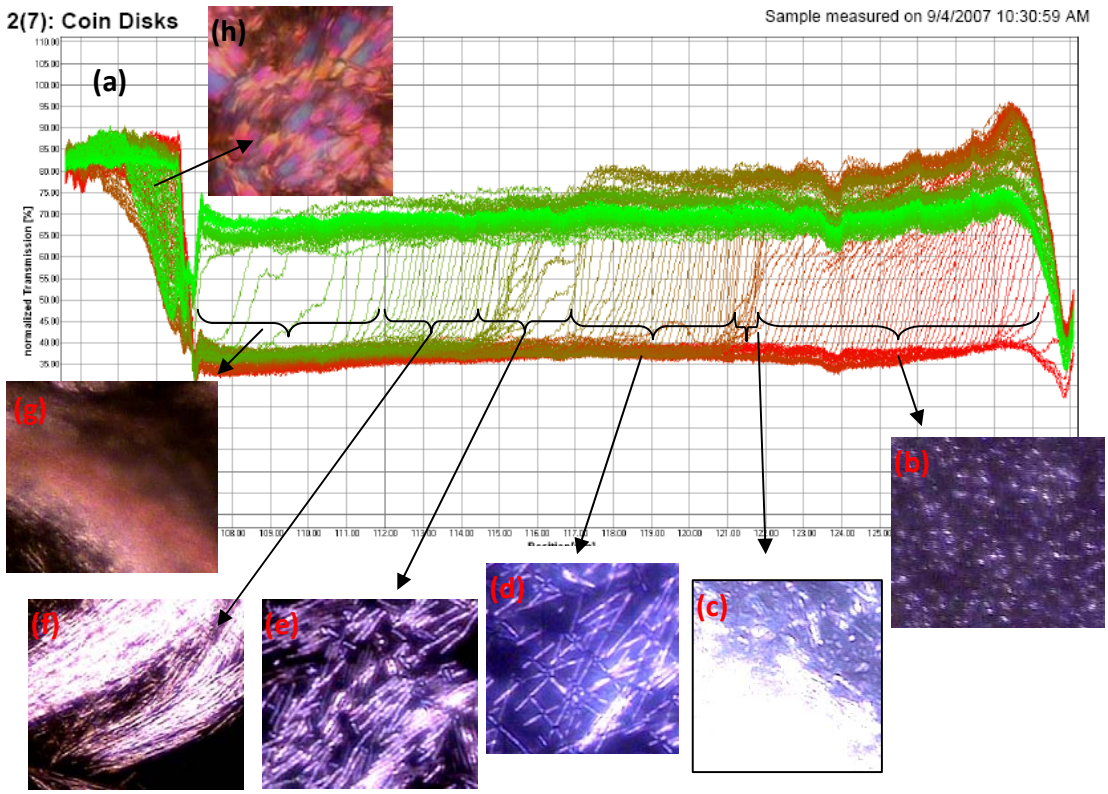

Picture taken from the author.

Figure 26. Coin like discotic system creaming in an analytical centrifugation machine.

The Figure shows the depletion attraction by increasing the coin-like disks concentration in the cuvette. **(a)** Transmission profile during the centrifugation. **(b)** Isotropic phase. **(c)** Cloud of disks. **(d)** Columnar phase right after the cloud was produced. **(e)** The rods intended to bundle. **(f)** The concentration of rods get higher and fully organized. (g) Some color starts to appear during the drying of the clouds of rods. **(h)** Beautiful colors shows up, looking like a possible liquid crystal of α-Eicosene.

The coin like disk system was stranger, many phase transitions were discovered (**Figure 26a**) and confirmed us what we initially saw during the evaporation of the water/ethanol drop discotic system. Seven possible phase transitions were found. The first one was the *Isotropic phase* (**Figure 26b**) phase, present in both cases.

The second phase was the transition of the Isotropic-Columnar phase (**Figure 26c**), but in this case, it look much more structured, as a cubic phase predicted by Frenkel using Monte Carlo simulations, but any accurate prove demonstrate it to us. The third one was the *Columnar phase* (**Figure 26d**). The fourth phase possibly wa the rods aligning each other (**Figure 26e**) and it created the fifth phase (**Figure 26f)**, which was the new colorful cloud, the ending of the drop evaporation but the initial stage of the *Liquid Crystal phase* (**Figure 26g**), which was the sixth phase and the hardest to explain.

The instrument gave us clues that our discotic systems were totally different and the depletion attraction, besides the amount of SDS in both systems were the same, it was totally different. We assumed if we leave two cuvettes for both systems alone for years, we possibly we will have the same results as we got in the analytical centrifugation machine.

Between the RBC colloidal disk system and the coin-like disk system, we could understand the huge difference in the self assembly of each one. Mean while the RBC cells disks stack much faster as the coin like disks, we could see the coin like disks organize much better than the RBC disks, letting to create very long rods and a very high organization of particles, which let us see possible crystals of α-Eicosene.

7. CONCLUSIONS

I. We have demonstrated the fabrication of uniform wax emulsions through electrospray. Using a stable cone-jet mode, spherical droplets of α-Eicosene with uniform size were obtained.

II. By tuning the flow rate and conductivity, suspensions of monodisperse wax particles with sizes ranging from 1 to 5 μm were obtained.

III. We found that the properties of collection solution, such as density and surface tension, were crucial to the formation of monodispersed suspensions. Discotic colloids were generated with this technique.

IV. We anticipate this novel emulsification method can be used in biomaterials development and drug delivery.

V. We have demonstrated the ability to mold phase changing emulsions by control the interface with the fluid in which they are suspended in using surfactants and co-surfactants.

VI. The molecules in the emulsion droplets oppose a special surface freezing transition and the packing of the interface molecules initiate the surface freezing and the layering prorogating inwards to complete the phase transition of the whole emulsion drop, and hence to change the shape from spherical to disk-like or possible other morphologies.

VII. The discotic systems agreed with Lekkerkerker's simulations, shown in the introduction, which told us that for disks with an aspect ratio of 1/5 a columnar phase was present, but for the RBC disks, which have an aspect ratio of 1/2 and

no simulations have not been done before, the columnar phase transition was very small and hard to get on it.

VIII. According to Lekkerkerker's and Frenkel's predictions, our two discotic system never will have a nematic phase due their aspect ratio (1/4 and 1/2 respectively), prediction that perfectly matched with our system

IX. By changing the SDS concentration of our samples we will be able to create a phase transition diagram using the LumiSizer instrument.

X. Such surface-bound sculpturing[105] of emulsion will have profound application in superparticle chemistry[106, 107].

XI. The RBC's disks system possibly will gain more money based on its analogies future studies on real human blood, but the coin-like disks had much more variety of phases and is more enthusiastic for scientists to understand its phase transition.

8. REFERENCES

1. Leich, M.A. and G.L. Richmond, *Recent experimental advances in studies of liquid/liquid interfaces.* Faraday Discussions, 2005. **129**: p. 1-21.
2. Carroll, B.J., *Physical Aspects of Detergency.* Colloids and Surfaces a-Physicochemical and Engineering Aspects, 1993. **74**(2-3): p. 131-167.
3. Herrera, C.G., *Detergency. Its main mechanisms.* Grasas Y Aceites, 1996. **47**(6): p. 419-435.
4. Wasan, D.T. and A.D. Nikolov, *Spreading of nanofluids on solids.* Nature, 2003. **423**(6936): p. 156-159.
5. Dreyfus, R., P. Tabeling, and H. Willaime, *Ordered and disordered patterns in two-phase flows in microchannels.* Physical Review Letters, 2003. **90**(14).
6. Stone, H.A., A.D. Stroock, and A. Ajdari, *Engineering flows in small devices: Microfluidics toward a lab-on-a-chip.* Annual Review of Fluid Mechanics, 2004. **36**: p. 381-411.
7. Anna, S.L. and H.C. Mayer, *Microscale tipstreaming in a microfluidic flow focusing device.* Physics of Fluids, 2006. **18**(12).
8. Bahr, C., *Surfactant-induced nematic wetting layer at a thermotropic liquid crystal/water interface.* Physical Review E, 2006. **73**(3).
9. Crawford, G.P., R.J. OndrisCrawford, and J.W. Doane, *Systematic study of orientational wetting and anchoring at a liquid-crystal-surfactant interface.* Physical Review E, 1996. **53**(4): p. 3647-3661.
10. Kou, X.S., et al., *One-step synthesis of large-aspect-ratio single-crystalline gold nanorods by using CTPAB and CTBAB surfactants.* Chemistry-a European Journal, 2007. **13**(10): p. 2929-2936.
11. Shylesh, S., et al., *One step synthesis of chromium-containing periodic mesoporous organosilicas and their catalytic activity in the oxidation of cyclohexane.* Microporous and Mesoporous Materials, 2007. **99**(3): p. 334-344.
12. Dugas, V., J. Broutin, and E. Souteyrand, *Droplet evaporation study applied to DNA chip manufacturing.* Langmuir, 2005. **21**(20): p. 9130-9136.
13. Wu, X.Z., et al., *Surface Crystallization of Liquid Normal-Alkanes.* Physical Review Letters, 1993. **70**(7): p. 958-961.
14. Lei, Q. and C.D. Bain, *Surfactant-induced surface freezing at the alkane-water interface.* Physical Review Letters, 2004. **92**(17).
15. Earnshaw, J.C. and C.J. Hughes, *Surface-Induced Phase-Transition in Normal Alkane Fluids.* Physical Review A, 1992. **46**(8): p. R4494-R4496.
16. Kambersky, H., *Base For Cosmetics*. 1965: United States.
17. Okoyama, N.A., Yoshihiko, *Wax emulsion*. 1984, Nippon Oil Co., Ltd. (Tokyo, JP): United States.
18. Claret, T.C.C., Wesley E.; Hodgson, Roy S., *Wax-based emulsions and their use in gypsum products*. 1997, Conoco Inc. (Ponca City, OK): United States.
19. Peek, B.M.S., Barry W.; Johnson, Roger Scott; DiCarlo, Daniel, *Composites prepared with ready-to-use resin/wax emulsion adhesives*. 2000, Georgia-Pacific Resins, Inc. (Atlanta, GA): United States.
20. Siegele, F.H., *Oil Well Fracturing Method Using Emulsions*. 1969, American Cyanamid Company: United States.
21. Joachim Lange, G., Otto Malitschek, Augsburg, and Fred Mader, *Method Of Improving Wax-containing Self-polishing Emulsions and Product*. 1972, Farbwerke Hoechst Aktiengesellschaft vormals Meister Lucius & Bruning: United States.
22. Hagenmaier, R.D. and R.A. Baker, *Wax Microemulsions and Emulsions as Citrus Coatings.* Journal of Agricultural and Food Chemistry, 1994. **42**(4): p. 899-902.

23. Zhang, Y.P., X.X. Hu, and X. Wang, *Theoretical analysis of convective heat transfer enhancement of microencapsulated phase change material slurries.* Heat and Mass Transfer, 2003. **40**(1-2): p. 59-66.
24. Charunyakorn, P., S. Sengupta, and S.K. Roy, *Forced-Convection Heat-Transfer in Microencapsulated Phase-Change Material Slurries - Flow in Circular Ducts.* International Journal of Heat and Mass Transfer, 1991. **34**(3): p. 819-833.
25. Mulligan, J.C., D.P. Colvin, and Y.G. Bryant, *Microencapsulated phase-change material suspensions for heat transfer in spacecraft thermal systems.* Journal of Spacecraft and Rockets, 1996. **33**(2): p. 278-284.
26. Montenegro, R. and K. Landfester, *Metastable and stable morphologies during crystallization of alkanes in miniemulsion droplets.* Langmuir, 2003. **19**(15): p. 5996-6003.
27. Shinohara, Y., et al., *Observation of the transient rotator phase of n-hexadecane in emulsified droplets with time-resolved two-dimensional small- and wide-angle x-ray scattering.* Physical Review Letters, 2005. **94**(9): p. 097801.
28. Herhold, A.B., H.E. King, and E.B. Sirota, *A vanishing nucleation barrier for the n-alkane rotator-to-crystal transformation.* Journal of Chemical Physics, 2002. **116**(20): p. 9036-9050.
29. Xie, B.Q., et al., *Crystallization behaviors of n-nonadecane in confined space: Observation of metastable phase induced by surface freezing.* Journal of Physical Chemistry B, 2006. **110**(29): p. 14279-14282.
30. Cheng, Z., P.M. Chaikin, and T.G. Mason, *Light streak tracking of optically trapped thin microdisks.* Physical Review Letters, 2002. **89**(10): p. 108303.
31. Luo, P. and Y.G. Gu, *Effects of asphaltene content on the heavy oil viscosity at different temperatures.* Fuel, 2007. **86**(7-8): p. 1069-1078.
32. Priyanto, S., G.A. Mansoori, and A. Suwono, *Measurement of property relationships of nano-structure micelles and coacervates of asphaltene in a pure solvent.* Chemical Engineering Science, 2001. **56**(24): p. 6933-6939.
33. Stefanini, M., et al., *Studies on Platelets .9. Observations on the Properties and Mechanism of Action of a Potent Platelet Agglutinin Detected in the Serum of a Patient with Idiopathic Thrombocytopenic Purpura (with a Note on the Pathogenesis of the Disease).* Blood, 1953. **8**(1): p. 26-64.
34. Hao, J.J., K.V. Subbarao, and J.M. Duniway, *Germination of Sclerotinia minor and S-sclerotiorum sclerotia under various soil moisture and temperature combinations.* Phytopathology, 2003. **93**(4): p. 443-450.
35. Pinel, F., E. Leclerc-Cessac, and S. Staunton, *Relative contributions of soil chemistry, plant physiology and rhizosphere induced changes in speciation on Ni accumulation in plant shoots.* Plant and Soil, 2003. **255**(2): p. 619-629.
36. van der Kooij, F.M., K. Kassapidou, and H.N.W. Lekkerkerker, *Liquid crystal phase transitions in suspensions of polydisperse plate-like particles.* Nature, 2000. **406**(6798): p. 868-871.
37. van der Kooij, F.M. and H.N.W. Lekkerkerker, *Formation of nematic liquid crystals in suspensions of hard colloidal platelets.* Journal of Physical Chemistry B, 1998. **102**(40): p. 7829-7832.
38. Petukhov, A.V., et al., *Observation of a hexatic columnar liquid crystal of polydisperse colloidal disks.* Physical Review Letters, 2005. **95**(7): p. 077801.
39. Morvan, M., et al., *Ultrasmall-Angle and Small-Angle X-Ray-Scattering of Smectite Clay Suspensions.* Colloids and Surfaces a-Physicochemical and Engineering Aspects, 1994. **82**(2): p. 193-203.
40. Zhang, L.M., et al., *Synchrotron SAXS/WAXD and rheological studies of clay suspensions in silicone fluid.* Journal of Colloid and Interface Science, 2003. **266**(2): p. 339-345.
41. Baird, J.C. and J.Y. Walz, *The effects of added nanoparticles on aqueous kaolinite suspensions I. Structural effects.* Journal of Colloid and Interface Science, 2006. **297**(1): p. 161-169.

42. Michot, L.J., et al., *Liquid-crystalline aqueous clay suspensions.* Proceedings of the National Academy of Sciences of the United States of America, 2006. **103**(44): p. 16101-16104.
43. Nicolai, T. and S. Cocard, *Dynamic light-scattering study of aggregating and gelling colloidal disks.* Journal of Colloid and Interface Science, 2001. **244**(1): p. 51-57.
44. Mongondry, P., J.F. Tassin, and T. Nicolai, *Revised state diagram of Laponite dispersions.* Journal of Colloid and Interface Science, 2005. **283**(2): p. 397-405.
45. Fossum, J.O., *Physical phenomena in clays.* Physica A, 1999. **270**(1-2): p. 270-277.
46. Saunders, A.E., et al., *Columnar self-assembly of colloidal nanodisks.* Nano Letters, 2006. **6**(12): p. 2959-2963.
47. Birch, H.M., *Down to the letter.* Nature, 2007. **446**(7138): p. 940-940.
48. Hernandez, C.J. and T.G. Mason, *Colloidal alphabet soup: Monodisperse dispersions of shape-designed LithoParticles.* Journal of Physical Chemistry C, 2007. **111**(12): p. 4477-4480.
49. Badaire, S., et al., *Shape selectivity in the assembly of lithographically designed colloidal particles.* Journal of the American Chemical Society, 2007. **129**(1): p. 40-41.
50. Baghdadi, H.A., H. Sardinha, and S.R. Bhatia, *Rheology and gelation kinetics in laponite dispersions containing poly(ethylene oxide).* Journal of Polymer Science Part B-Polymer Physics, 2005. **43**(2): p. 233-240.
51. Knaebel, A., et al., *Aging behavior of Laponite clay particle suspensions.* Europhysics Letters, 2000. **52**(1): p. 73-79.
52. Fossum, J.O., et al., *Self-affine crossover length in a layered silicate deposit.* Physical Review E, 2004. **69**(3): p. 036108.
53. Wilding, N.B., et al., *Phase behavior and particle size cutoff effects in polydisperse fluids.* Journal of Chemical Physics, 2006. **125**(1): p. 01490.
54. Adams, M. and S. Fraden, *Phase behavior of mixture's of rods (tobacco mosaic virus) and spheres (polyethylene oxide, bovine serum albumin).* Biophysical Journal, 1998. **74**(1): p. 669-677.
55. Urakami, N. and M. Imai, *Dependence on sphere size of the phase behavior of mixtures of rods and spheres.* Journal of Chemical Physics, 2003. **119**(4): p. 2463-2470.
56. Fasolo, M. and P. Sollich, *Effects of colloid polydispersity on the phase behavior of colloid-polymer mixtures.* Journal of Chemical Physics, 2005. **122**(7): p. 074904.
57. Sollich, P., *Predicting phase equilibria in polydisperse systems.* Journal of Physics-Condensed Matter, 2002. **14**(3): p. R79-R117.
58. Germain, V. and M.P. Pileni, *Size distribution of cobalt nanocrystals: A key parameter in formation of columns and labyrinths in mesoscopic structures.* Advanced Materials, 2005. **17**(11): p. 1424-+.
59. Kofke, D.A. and P.G. Bolhuis, *Freezing of polydisperse hard spheres.* Physical Review E, 1999. **59**(1): p. 618-622.
60. Wensink, H.H. and G.J. Vroege, *Isotropic-nematic phase behavior of length-polydisperse hard rods.* Journal of Chemical Physics, 2003. **119**(13): p. 6868-6882.
61. Clarke, N., et al., *Phase equilibria in the polydisperse Zwanzig model of hard rods.* Journal of Chemical Physics, 2000. **113**(14): p. 5817-5829.
62. Veerman, J.A.C. and D. Frenkel, *Phase-Diagram of a System of Hard Spherocylinders by Computer-Simulation.* Physical Review A, 1990. **41**(6): p. 3237-3244.
63. Bates, M.A. and D. Frenkel, *Influence of polydispersity on the phase behavior of colloidal liquid crystals: A Monte Carlo simulation study.* Journal of Chemical Physics, 1998. **109**(14): p. 6193-6199.
64. van der Kooij, F.M., D. van der Beek, and H.N.W. Lekkerkerker, *Isotropic-nematic phase separation in suspensions of polydisperse colloidal platelets.* Journal of Physical Chemistry B, 2001. **105**(9): p. 1696-1700.
65. van der Kooij, F.M. and H.N.W. Lekkerkerker, *Liquid-crystal phase transitions in suspensions of plate-like particles.* Philosophical Transactions of the Royal Society of

London Series a-Mathematical Physical and Engineering Sciences, 2001. **359**(1782): p. 985-995.
66. Wensink, H.H., G.J. Vroege, and H.N.W. Lekkerkerker, *Isotropic-nematic density inversion in a binary mixture of thin and thick hard platelets.* Journal of Physical Chemistry B, 2001. **105**(43): p. 10610-10618.
67. Bates, M.A. and D. Frenkel, *Nematic-isotropic transition in polydisperse systems of infinitely thin hard platelets.* Journal of Chemical Physics, 1999. **110**(13): p. 6553-6559.
68. Mason, T.G., *Osmotically driven shape-dependent colloidal separations.* Physical Review E, 2002. **66**(6-1): p. 060402.
69. Deng, W.W., et al., *Increase of electrospray throughput using multiplexed microfabricated sources for the scalable generation of monodisperse droplets.* Journal of Aerosol Science, 2006. **37**(6): p. 696-714.
70. Tang, K.Q. and A. Gomez, *Monodisperse electrosprays of low electric conductivity liquids in the cone-jet mode.* Journal of Colloid and Interface Science, 1996. **184**(2): p. 500-511.
71. Fantini, D., M. Zanetti, and L. Costa, *Polystyrene microspheres and nanospheres produced by electrospray.* Macromolecular Rapid Communications, 2006. **27**(23): p. 2038-2042.
72. Roh, K.H., D.C. Martin, and J. Lahann, *Biphasic Janus particles with nanoscale anisotropy.* Nature Materials, 2005. **4**(10): p. 759-763.
73. Fenn, J.B., et al., *Electrospray Ionization for Mass-Spectrometry of Large Biomolecules.* Science, 1989. **246**(4926): p. 64-71.
74. Chen, X.P., et al., *Spraying modes in coaxial jet electrospray with outer driving liquid.* Physics of Fluids, 2005. **17**(3): p. 032101.
75. Loscertales, I.G., et al., *Micro/nano encapsutation via electrified coaxial liquid jets.* Science, 2002. **295**(5560): p. 1695-1698.
76. Yeo, L.Y., Z. Gagnon, and H.C. Chang, *AC electrospray biomaterials synthesis.* Biomaterials, 2005. **26**(31): p. 6122-6128.
77. Kyritsis, D.C., et al., *Optimization of a catalytic combustor using electrosprayed liquid hydrocarbons for mesoscale power generation.* Combustion and Flame, 2004. **139**(1-2): p. 77-89.
78. Barrero, A., et al., *Steady cone-jet electrosprays in liquid insulator baths.* Journal of Colloid and Interface Science, 2004. **272**(1): p. 104-108.
79. Bocanegra, R., et al., *Production of cocoa butter microcapsules using an electrospray process.* Journal of Food Science, 2005. **70**(8): p. E492-E497.
80. Bocanegra, R., et al., *Multiple electrosprays emitted from an array of holes.* Journal of Aerosol Science, 2005. **36**(12): p. 1387-1399.
81. Adams, M., et al., *Entropically driven microphase transitions in mixtures of colloidal rods and spheres.* Nature, 1998. **393**(6683): p. 349-352.
82. Dogic, Z. and S. Fraden, *Ordered phases of filamentous viruses.* Current Opinion in Colloid & Interface Science, 2006. **11**(1): p. 47-55.
83. Livolant, F., et al., *The Highly Concentrated Liquid-Crystalline Phase of DNA Is Columnar Hexagonal.* Nature, 1989. **339**(6227): p. 724-726.
84. Hitt, A.L., A.R. Cross, and R.C. Williams, *Microtubule Solutions Display Nematic Liquid-Crystalline Structure.* Journal of Biological Chemistry, 1990. **265**(3): p. 1639-1647.
85. Davidson, P. and J.C.P. Gabriel, *Mineral liquid crystals.* Current Opinion in Colloid & Interface Science, 2005. **9**(6): p. 377-383.
86. Wiley, B., et al., *Shape-controlled synthesis of metal nanostructures: The case of silver.* Chemistry-a European Journal, 2005. **11**(2): p. 454-463.
87. Ren, J.T. and R.D. Tilley, *Preparation, self-assembly, and mechanistic study of highly monodispersed nanocubes.* Journal of the American Chemical Society, 2007. **129**(11): p. 3287-3291.
88. Kim, J.W., R.J. Larsen, and D.A. Weitz, *Synthesis of nonspherical colloidal particles with anisotropic properties.* Journal of the American Chemical Society, 2006. **128**(44): p. 14374-14377.

89. Li, X., T.J. Wang, and Y. Jin, *Granulation process for producing spherical particles of a rubber antioxidant in a water cooling tower.* Chemical Engineering & Technology, 2006. **29**(10): p. 1273-1280.
90. Li, Z.X., et al., *The Structure of the Surface of Ethanol-Water Mixtures.* Molecular Physics, 1993. **80**(4): p. 925-939.
91. Daniel, R.C. and J.C. Berg, *Dynamic surface tension of polydisperse surfactant solutions: A pseudo-single-component approach.* Langmuir, 2002. **18**(13): p. 5074-5082.
92. Gang, H., et al., *Rotator phases and surface crystallization in alpha-eicosene.* Journal of Physical Chemistry B, 1998. **102**(15): p. 2754-2758.
93. Samsel, R.W. and A.S. Perelson, *Kinetics of Rouleau Formation .1. a Mass-Action Approach with Geometric Features.* Biophysical Journal, 1982. **37**(2): p. 493-514.
94. Samsel, R.W. and A.S. Perelson, *Kinetics of Rouleau Formation .2. Reversible-Reactions.* Biophysical Journal, 1984. **45**(4): p. 805-824.
95. Thorsen, T., et al., *Dynamic pattern formation in a vesicle-generating microfluidic device.* Physical Review Letters, 2001. **86**(18): p. 4163-4166.
96. Utada, A.S., et al., *Monodisperse double emulsions generated from a microcapillary device.* Science, 2005. **308**(5721): p. 537-541.
97. Tulpar, A. and W.A. Ducker, *Surfactant adsorption at solid-aqueous interfaces containing fixed charges: Experiments revealing the role of surface charge density and surface charge regulation.* Journal of Physical Chemistry B, 2004. **108**(5): p. 1667-1676.
98. Asakura, S. and F. Oosawa, *On Interaction between 2 Bodies Immersed in a Solution of Macromolecules.* Journal of Chemical Physics, 1954. **22**(7): p. 1255-1256.
99. Spicer, P.T. and R.W. Hartel, *Crystal comets: Dewetting during emulsion droplet crystallization.* Australian Journal of Chemistry, 2005. **58**(9): p. 655-659.
100. Backstrom, K., B. Lindman, and S. Engstrom, *Removal of Triglycerides from Polymer Surfaces in Relation to Surfactant Packing - Ellipsometry Studies.* Langmuir, 1988. **4**(4): p. 872-878.
101. Vollhardt, D. and G. Emrich, *Coadsorption of sodium dodecyl sulfate and medium-chain alcohols at the air-water interface.* Colloids and Surfaces a-Physicochemical and Engineering Aspects, 2000. **161**(1): p. 173-182.
102. Vollhardt, D., et al., *Phase transition in adsorbed monolayers of sodium dodecyl sulfate/dodecanol mixtures.* Journal of Physical Chemistry B, 2001. **105**(48): p. 12061-12067.
103. Wantke, K.D., H. Fruhner, and J. Ortegren, *Surface dilatational properties of mixed sodium dodecyl sulfate/dodecanol solutions.* Colloids and Surfaces a-Physicochemical and Engineering Aspects, 2003. **221**(1-3): p. 185-195.
104. Veerman, J.A.C. and D. Frenkel, *Phase-Behavior of Disk-Like Hard-Core Mesogens.* Physical Review A, 1992. **45**(8): p. 5632-5648.
105. Ward, A.D., et al., *Optical sculpture: controlled deformation of emulsion droplets with ultralow interfacial tensions using optical tweezers.* Chemical Communications, 2006(43): p. 4515-4517.
106. Nelson, D.R., *Toward a tetravalent chemistry of colloids.* Nano Letters, 2002. **2**(10): p. 1125-1129.
107. Edwards, E.W., D.Y. Wang, and H. Mohwald, *Hierarchical organization of colloidal particles: From colloidal crystallization to supraparticle chemistry.* Macromolecular Chemistry and Physics, 2007. **208**(5): p. 439-445.

ATTACHMENT 1. Electrospray of Low Electric Conductivity Liquids

Electrostatic liquid atomization is a process that relies on electrostatic forces to break the liquid into fine charged droplets. One of the simplest ways to implement such a process is to feed a liquid sufficient electric conductivity into a metal capillary charged at a sufficiently high electric potential relative to a ground electrode a few centimeters away. The liquid is often observed to form a conical meniscus at the outlet of the capillary, through the apex of which a fine liquid ligament is ejected. The liquid ligament breaks up farther downstream to disperse into a spray of droplets which often shows a remarkably narrow size distribution.

The effects of liquid flow rate, applied voltage and liquid electric conductivity on droplet size and spray monodispersity has been investigated before. The droplet size is dominantly controlled by the liquid flow rate and secondarily by the applied voltage. Is has no dependency on the capillary size. Some properties of a low electric conductivity liquid are mentioned in **Table 1**.

Liquid Physical Properties

Liquid solution	Electric conductivity, k (1/Ω cm)	Surface tension, σ (dyn/cm)	Kinematic viscosity, ν (cm^2/s)	Dielectric constant, ϵ
0.1% Stadis 450	7.3×10^{-9}	18.6	6.12×10^{-3}	1.94
0.3% Stadis 450	1.4×10^{-8}	18.6	6.15×10^{-3}	1.93
0.6% Stadis 450	2.3×10^{-8}	18.6	6.12×10^{-3}	1.93
1.2% Stadis 450	4.1×10^{-8}	18.6	6.16×10^{-3}	1.92
2.0% Stadis 450	6.7×10^{-8}	18.7	6.26×10^{-3}	1.91
2.5% Stadis 450	8.3×10^{-8}	18.5	6.30×10^{-3}	1.91
3.0% Stadis 450	9.8×10^{-8}	18.6	6.35×10^{-3}	1.90

Table taken from Keqi Tang and Alessandro Gomez.

Table 1. Influence of some properties using STADIS 450.

The influence inside the Electric Conductivity and other properties by using STADIS 450 in a low electric conductivity liquid.

The applied voltage is certainly a key variable in establishing the cone-jet mode. Despite this crucial role, droplet size was reported to be virtually independent of the applied voltage for liquid of relatively high electric conductivity.

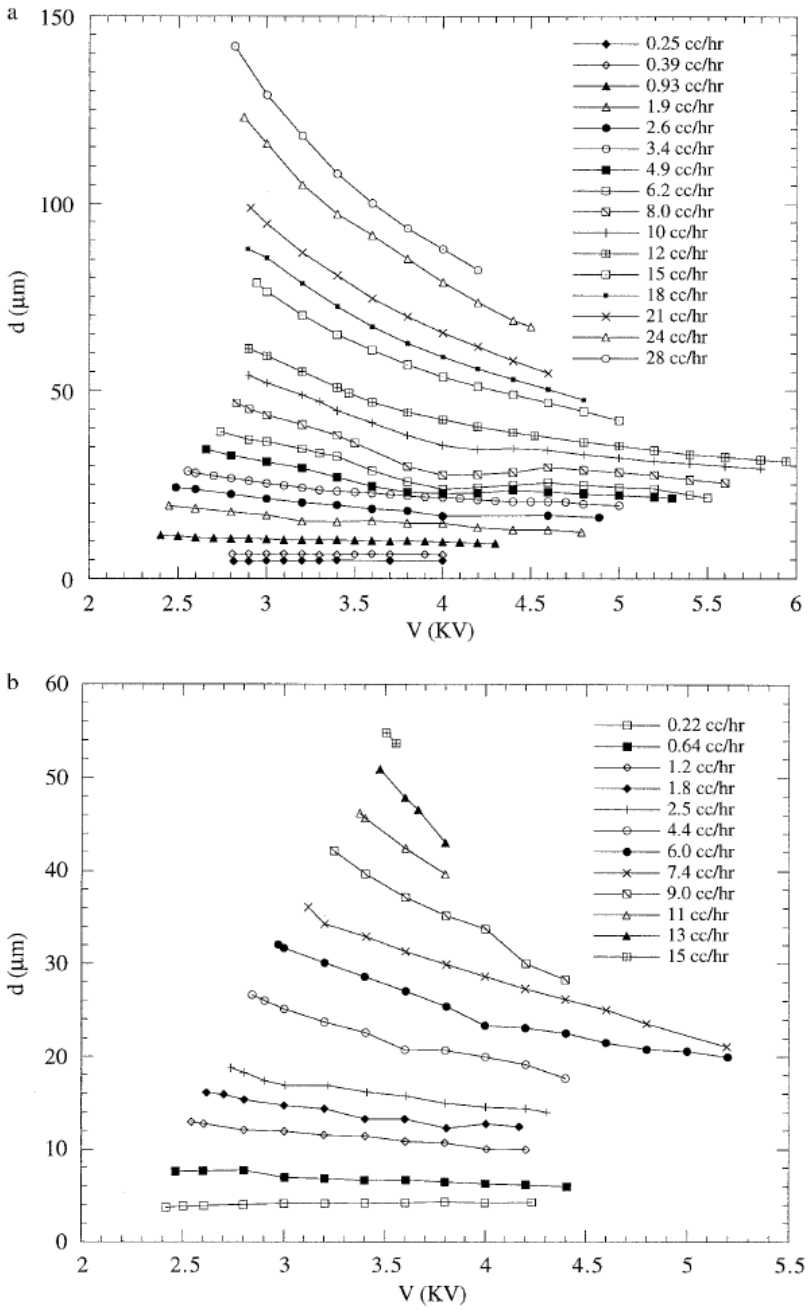

Figures taken from Keqi Tang and Alessandro Gomez.

Figure 27. Droplet diameter vs voltage.

Droplet diameter vs voltage applied to the capillary for two heptane solutions at different flow rates: (a) heptane / 0.3% Stadis 450; (b) heptane / 2.0% Stadis 450.

At low flow rates, the voltage seems to have a modest effect, if any. At larger flow rates, on the other hand, the droplet size decreases monotonically with the increase of the applied voltage and its effect appears to be more pronounced for the low conductivity solutions. (**Figure 27**.).

As the applied voltage was increased, the liquid cone was observed to shrink toward the capillary and the angle of the cone increased.

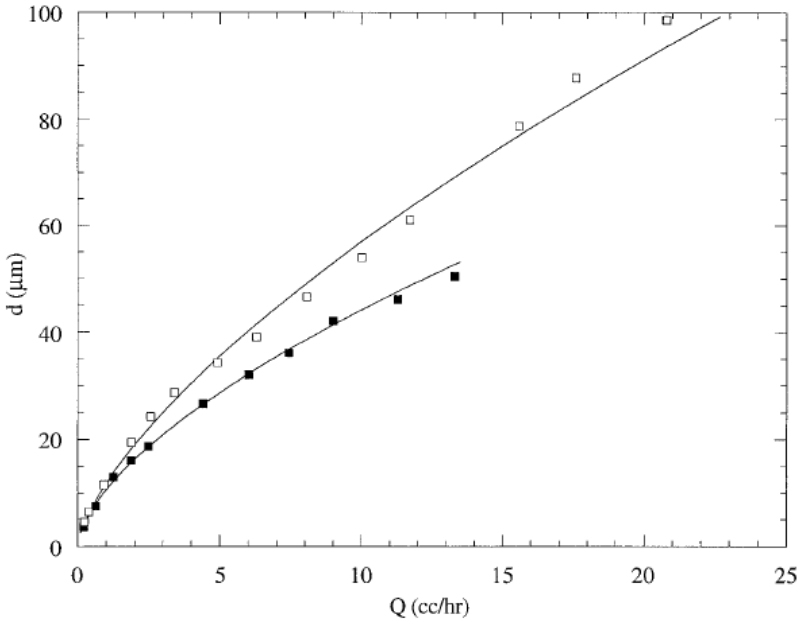

Figure taken from Keqi Tang and Alessandro Gomez.

Figure 28. Droplet mean diameter vs liquid flow rate at onset voltage.

Droplet mean diameter vs liquid flow rate at onset voltage conditions for heptane / 0.3% Stadis 450 (open symbols) and heptane / 2% Stadis 450 (solid symbols).

Droplet size dependence on liquid flow rate for two solutions of different conductivities. The electrospray was operated at the onset voltage conditions, defined here as the minimum voltage required for a cone-jet spray. The droplet size increases monotonically with the liquid flow. (**Figure 28**.).

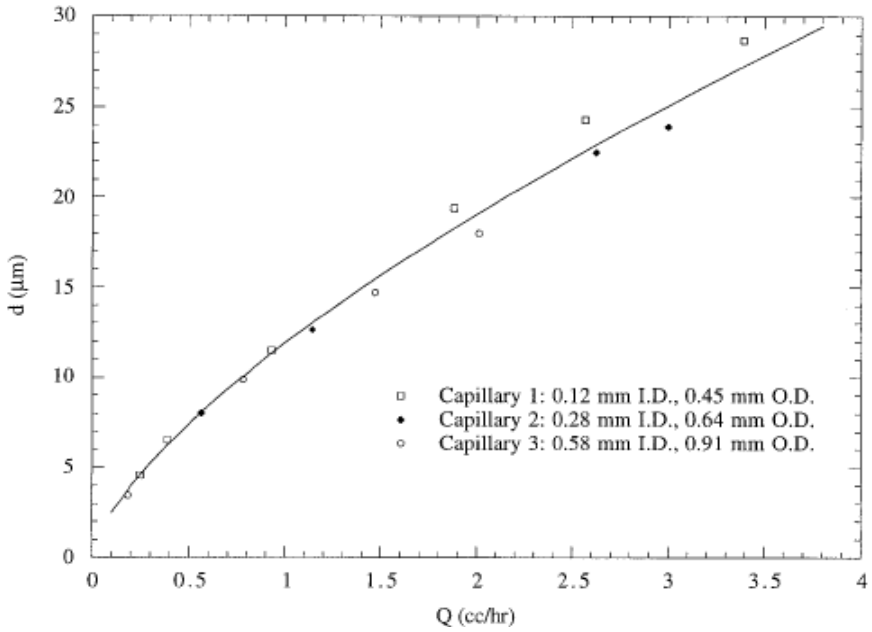

Figure taken from Keqi Tang and Alessandro Gomez.

Figure 29. Droplet mean diameter vs liquid flow rate at onset voltage for different capillary sizes.

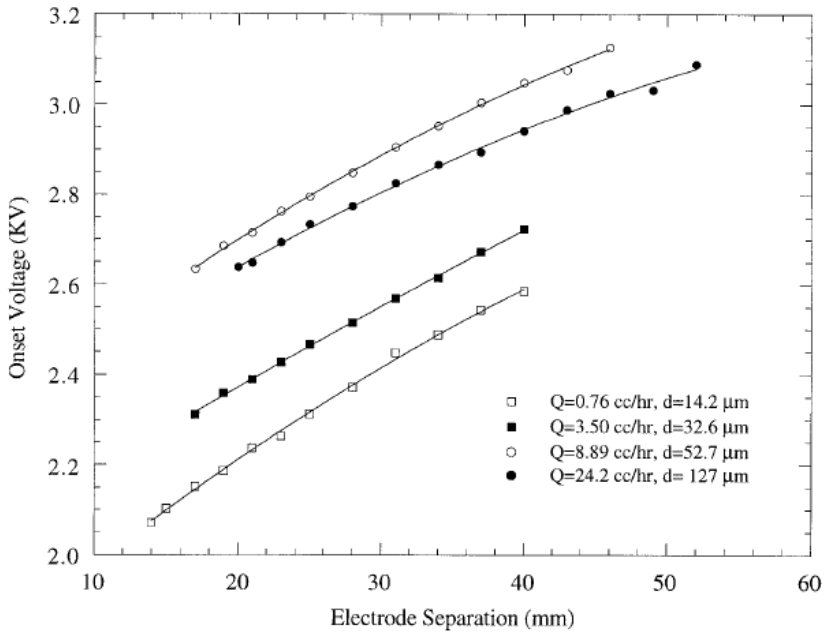

Figure taken from Keqi Tang and Alessandro Gomez.

Figure 30. Onset voltage plotter as a function of the distance between the capillary and the ground plate.

Onset voltage plotted as a function of the distance between the capillary and the ground plate for heptane / 0.3% Stadis 450.

The **figure 29** and **30** suggests that, once the cone-jet mode is established, the droplet size is independent of the geometric dimensions of the electrodes. It also implies that the onset condition of a cone-jet electrospray depends only on the electric field at the ligament which is affected by the combination of the applied voltage and the electrode separation.

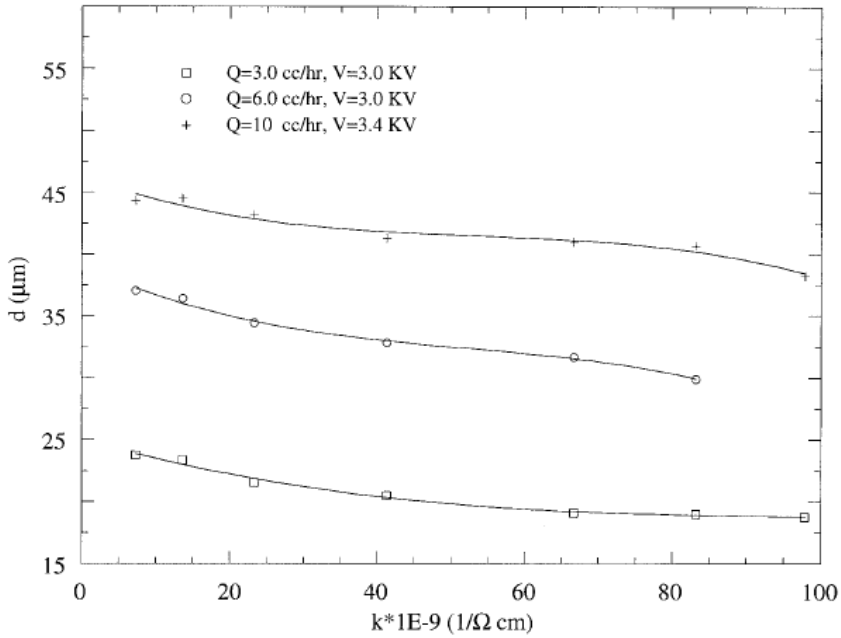

Figure taken from Keqi Tang and Alessandro Gomez.

Figure 31. Droplet mean diameter vs electric conductivity.

Droplet mean diameter vs electric conductivity of heptane at different liquid flow rates and selected voltages.

At a fixed flow rate and applied voltage, an increase of liquid conductivity by one order of magnitude decreases the size of the droplet by about 15% (**Figure 31**.). Similar results can also be found for sprays operating at fixed liquid flow rate and different voltages.

ATTACHMENT 2. The effect of Cosurfactans in α-Eicosene Rotator Phases and Surface Crystallization

Recent studies of the adsorbed monolayers of single component surfactants dissolved in aqueous solutions have shown that formation and development of a condensed phase is subjected to conditions similar to those in Langmuir monolayers where, after the main phase transition, the condensed phase is in coexistence with the initial fluidlike phase.

The question arose whether a first-order phase transition can also occur with the coadsorption of dissolved SDS/dodecanol mixtures containing dodecanol only as minor component.

Fundamental differences in the adsorption properties exist between the single components of the SDS/dodecanol mixture. The adsorbed monolayer of highly purified SDS does not show a phase transition even above the CMC and at low temperature so that condensed phase domains cannot be formed. The adsorbed monolayer of pure dodecanol has, in contrast to SDS, the characteristic features for a first-order phase transition during the adsorption kinetics. This provides good preconditions for studying the coadsorption of SDS and dodecanol in trace amounts from aqueous solutions.

The present experimental studies of the $\pi(t)$ adsorption kinetics (**Figures 32 and 33**) support the previous results and indicate a main phase transition over the measured temperature region and for different dodecanol concentrations. **Figure 32** shows the dynamic surface pressure for the 15 μM dodecanol/3 mM SDS mixture at 5, 10, and 15 °C and **Figure 33** for the 10 μM dodecanol/3 mM SDS mixture at the same temperatures.

In all cases, the surface pressure increases very quickly so that at the first beginning of the measurements it is already at the level of the equilibrium adsorption for the pure SDS solution.

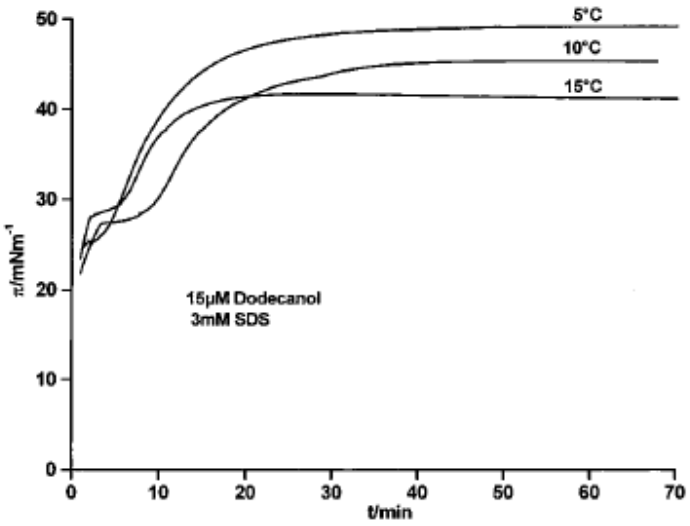

Figure taken from D. Vollhardt and G. Emrich.

Figure 32. π(*t*) adsorption curves with a first-order phase transition obtained for coadsorption.

π(*t*) adsorption curves with a first-order phase transition obtained for coadsorption from a 15 μM dodecanol/3 mM SDS solution at different temperatures. The break point in the slope indicates the first-order phase transition.

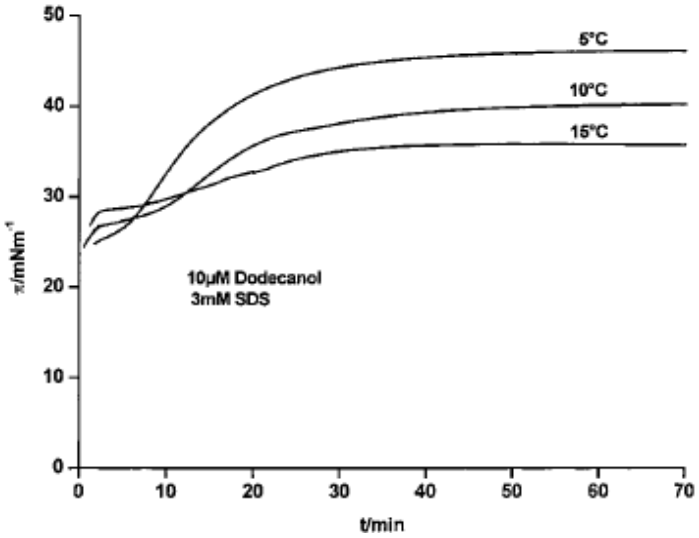

Figure taken from D. Vollhardt and G. Emrich.

Figure 33. π(t) adsorption curves with a first-order phase transition obtained for coadsorption.

π(t) adsorption curves with a first-order phase transition obtained for coadsorption from a 10 µM dodecanol/3 mM SDS solution at different temperatures. The break point in the slope indicates the first-order phase transition.

For the selected temperatures and dodecanol concentrations, all curves show a conspicuous break point in the continuous course of the adsorption kinetics curves, i.e., at these conditions a first order phase transition takes place in the adsorbed monolayer of the SDS/dodecanol mixtures. The surface pressure of the phase transition point depends on the temperature. For a selected SDS/dodecanol mixture ratio, the surface pressure of the phase transition point increases with increasing temperature but the differences are comparatively small to those observed for the adsorption kinetics of the single component dodecanol at the same concentrations in the aqueous subphase.

The coadsorption of the second component SDS causes the reduced temperature dependence of the phase transition point of the surface pressure. The π(*t*) adsorption curves are similar in shape after the phase transition point, despite quantitative differences depending on the dodecanol concentration of the aqueous

solution and on temperature (**Figures 32 and 33**). A region with a small pressure increase is followed by a time interval with a comparatively steep pressure increase, which quickly levels out at the equilibrium pressure. The equilibrium pressure of the dissolved SDS/ dodecanol mixtures increases with decrease of temperature and increase of the dodecanol concentration of the bulk solution.

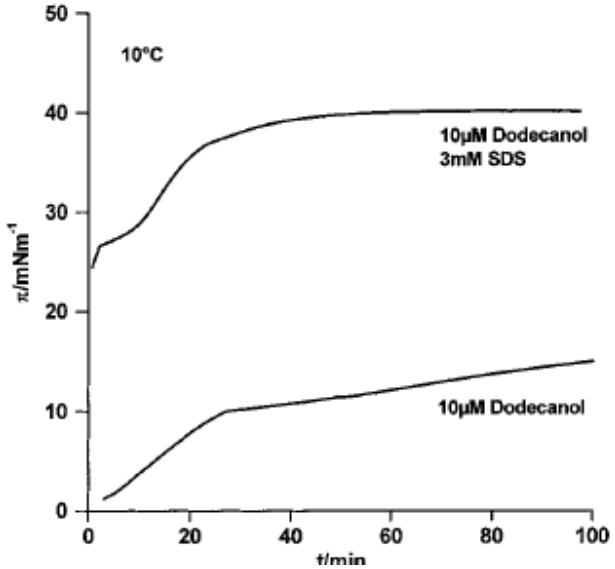

Figure taken from D. Vollhardt and G. Emrich.

Figure 34. Comparison of the π(*t*) adsorption curves.

Comparison of the π(*t*) adsorption curves of the singlecomponent 10 µM dodecanol solution (lower line) and of the mixed 10 µM dodecanol/3 mM SDS solution (upper line) at 10 °C. The first order phase transition indicated in both systems by the break point takes place in the mixed solution (2 min) after a much shorter time than for the single-component dodecanol solution (28 min) at the same concentration.

As seen in **Figure 34**, the dodecanol adsorption affects the surface pressure at an earlier stage of the adsorption process than does the pure dodecanol solution. This experimental finding has also been corroborated by a theoretical analysis of the mixed system according to which the critical adsorption value characteristic for the first-order phase transition decreases for the mixed solution. A comparable phenomenon is the effect of the penetration of dissolved surfactants on the phase transition in Langmuir monolayers, in the course of which the phase transition point

is shifted to lower surface concentrations, i.e., to higher values of the molecular area.

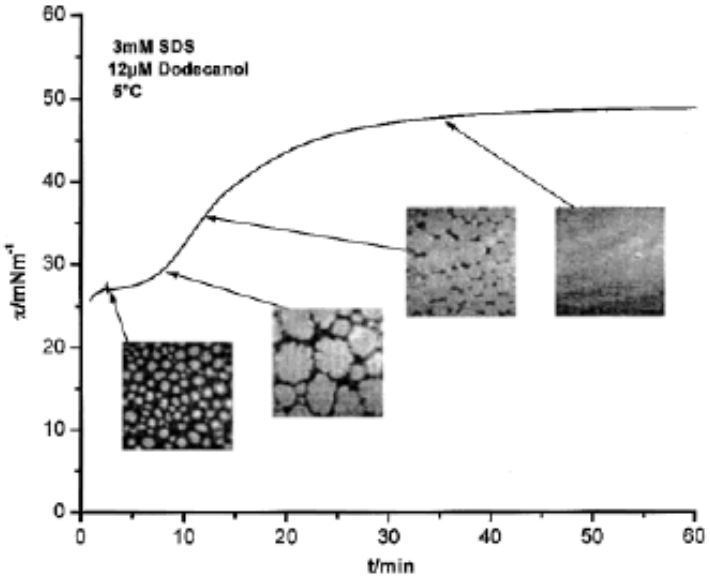

Figure taken from D. Vollhardt and G. Emrich.

Figure 35. π(t) coadsorption.

π(t) coadsorption from an aqueous 12 *µ*M dodecanol/3 mM SDS solution and the corresponding BAM images at the indicated times. All images have the same scale of 325 *µ*m x 325 *µ*m.

Figure 35 demonstrates the situation during the quick pressure increase region. Here coalescence of the domains takes place increasingly filling the gaps between them. Finally, near the equilibrium pressure they approach an almost homogeneous condensed film. The morphological behavior of the condensed phase domains formed after the main phase transition point resembles that observed for the adsorbed monolayers of pure dodecanol solutions.

ATTACHMENT 3. Surfactant adsorption at Solid-Aqueous Interfaces Containing Fixed Charges.

Surfactant adsorption is widely used to achieve changes in wetting, colloidal properties, and lubrication. Many surfactants are charged, and it is well-known that the charge on the solid-liquid interface affects the amount of adsorption, the shape of the adsorption isotherm, and the organization of the adsorbed surfactant molecules. The adsorption of cationic surfactants to solid-aqueous interfaces has recently been reviewed. However, to date there has not been a study of the adsorption of surfactants in which the magnitude and or the distribution of surface charges has been controlled independently of the surfactant adsorption (**Figure 36**.).

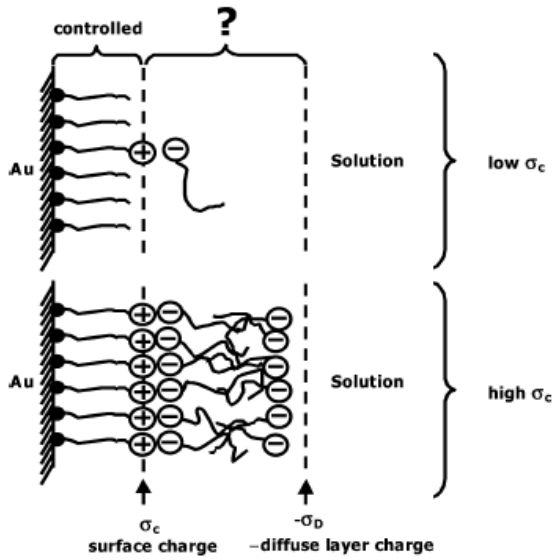

Figure taken from Aysen Tulpar and William A. Ducker.

Figure 36. Model for surface charge density and surfactant adsorption.

The black spheres, the positively charged headgroups, and the negatively charged headgroups represent -S, -N+(CH3)3, and -OSO3 -, respectively.

The reason is that for most solid-liquid interfaces the interfacial charge is not fixed but is regulated by adsorption and desorption of ions, including the surfactant ions.

Surfactant adsorption is also controlled by forces acting on the hydrophobic tail. There is often a concentration range where the surface excess of surfactant increases rapidly with concentration. This is known as the hemimicelle concentration, and there is evidence to support the idea that the acceleration in adsorption is due to a decrease in the amount of water in contact with the alkyl chains. The energy decrease through partial or full removal of the alkyl chain from the aqueous environment is often enough to overcome the energy penalty of charging the surface.

One critical role of charge regulation is therefore to suppress the electrostatic penalty for adsorption until the surfactant density is high enough to allow many lateral interactions between the surfactant tails. This enables hemimicelle formation at low concentrations. Implicit in most ideas of charge regulation is the idea that charges are free to migrate across the surface. Thus, a charge-regulating surface facilitates adsorption of a cluster of surfactant molecules through the creation of a cluster of surface charges on *neighboring* surface sites.

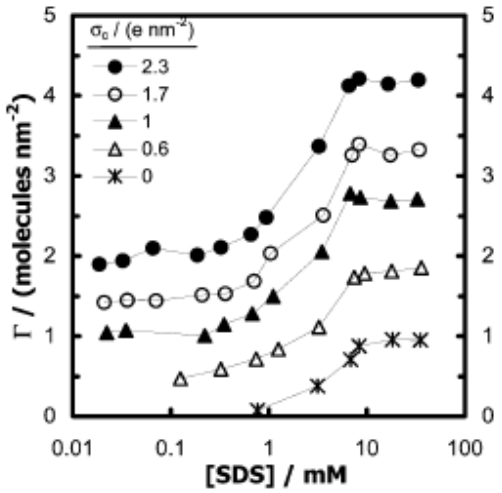

Figure taken from Aysen Tulpar and William A. Ducker.

Figure 37. Adsorption of SDS to a series of SAMs of fixed surface charge.

The figure shows the adsorption of SDS from aqueous solution to SAMs of various surface charge densities.

ATTACHMENT 4. Characterization of Colloidal Dispersion by Analytical Centrifugation.

Application of nanoparticles in diverse fields is fast developing. For practical applications, the colloidal stability of nanoparticle dispersions and the particle size distribution is of paramount importance. This relates to the need for a high through-put tool for the analysis of the dispersion properties during formulation, selection of processing conditions and for quality control of manufactured batches.

The phase behavior of nanoparticle dispersions and the phenomenon of colloidal crystallization is closely related to the nature of particle interactions and particle polydispersity, i.e. colloidal crystallization is favoured by a low degree of particle aggregation and low polydispersity of particle size.

The thesis describes the application of multisample analytical centrifugation for qualitative and quantitative characterization of nanoparticle suspensions.

Picture taken from Lumisizer manual.

Figure 38. Lumisizer instrument picture.

Lumisizer Centrifugation instrument.

The multisample analytical centrifuge (LUMiFuge, LUM GmbH, Berlin-Germany), **Figure 38**, used in this study, employs the STEP techonology, which allows to measure the intensity of the transmitted light as function of time and position over the entire sample length simultaneously, as shown in **Figure 39**.

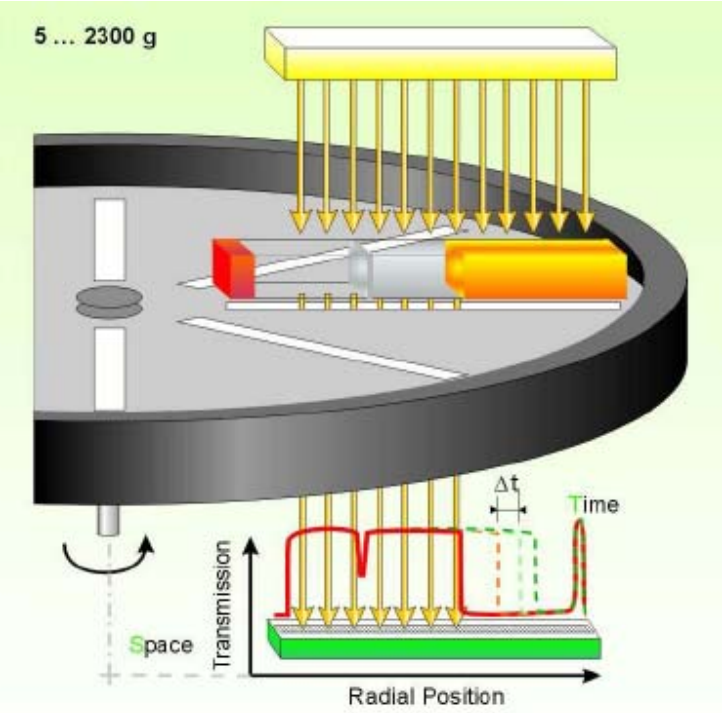

Figure taken from Lumisizer manual.

Figure 39. Measurement scheme of the multisample analytical photocentrifuge.

Parallel NIR-light is passed through the sample cells and the distribution of local transmission is recorded at preset time intervals over the entire sample length

The data are displayed as function of the position within the sample, as distance from the center of rotation (transmission, profiles, see **Figure 40**). The progression of the transmission profiles contains the information on the kinetics of separation process and allows particle characterization. The transmission profiles are representative for the variation of particle concentration inside the sample (low transmission means high particles concentration and vice versa). On the other hand, transmission profiles also reflected changes in the optical properties of the dispersions.

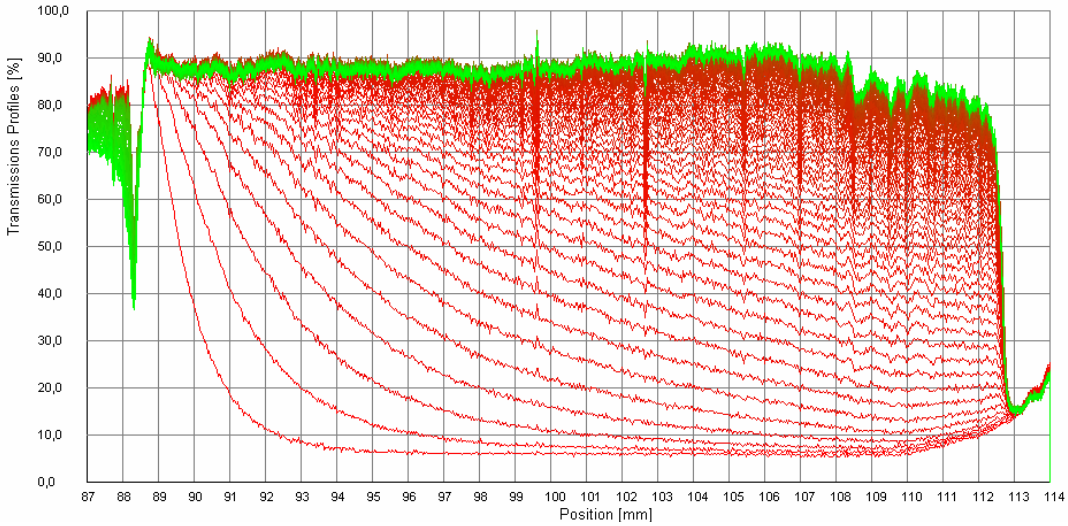

Figure taken from Lumisizer manual.

Figure 40. Transmission profiles using Lumisizer.

Evolution of transmission profiles during centrifugation – first recorded profiles undermost (red), last profiles uppermost (green), profiles measured every ten seconds. The sharp insection in the transmission profiles above 88 mm corresponds to the filling height of the sample. The position of the cell bottom is approx. at 114 mm.

At the same time, up to 8 different samples can be analyzed simultaneously at constant or variable centrifugal speed up to 2300g. The separation and crystallization behavior of the individual samples can be compared and analyzed in detail by tracing the variation in the transmission at any part of the sample or by tracing the movement of any phase boundary.

ATTACHMENT 5. The basis of the Polarization Microscope.

Due to the Brownian thermal forces, microdisks are fluctuating in different orientations. For observing the wax microdisks in our laboratory, an inverted polarized light microscope (Nikon TE2000-U) was used. **Figure 41** demonstrates the configuration of the inverted polarized light microscope. The polarized light microscope can distinguish between isotropic and anisotropic materials, and investigate the structure and composition of materials.

Isotropic materials demonstrate the same optical properties in all directions, as they have only one refractive index and allow all vibration directions of light passing through them. When light enters an isotropic material, it is refracted at a constant angle and passes through the material at a single velocity without being polarized by interaction with the electronic components of the crystalline lattice. On the other hand, anisotropic materials have crystallographically distinct axes and act as beam splitters. Also they interact with light in a manner that is dependent upon the orientation of the crystalline lattice with respect to the incident light. When light enters along the optical axis of anisotropic crystals, light is refracted at a constant angle and passes through the material at a single velocity, which has the manner as the interaction with isotropic materials. However, when light enters a non-equivalent axis, it is refracted into two rays, which are polarized, orientated at right angles to one another, and traveled at different velocities. This is called double refraction.

Polarized light microscope consists of two polarizing filters in the light path called polarizer and analyzer, as shown in **Figure 41**. When both the polarizer and analyzer are in the optical path, their polarization directions are positioned at a certain angle to each other. When the polarizer and analyzer are crossed at right

angles to each other and an isotropic media is between them, no light is passing through the system and a dark field of view present in the eye piece.

When normal light rays first pass through the polarizer, part of the light rays will be absorbed, and the transmitted light rays will be polarized, meaning light only vibrates at one single direction. **Figure 42** demonstrates the light rays passing through the birefringent material under the polarized light microscope. The transmitted light rays then pass through the anisotropic crystal where light rays are refracted and divided into two different components which are vibrating parallel to the crystallographic axes and perpendicular to each other. That is because the liquid crystal molecules have their own orientations and alignments; they observed differently of the light ray. Depending on the phases or the molecules' orientations of liquid crystals, the polarization of the transmitted light rays will be altered again after passing through the liquid crystals. The polarized light rays after passing through the birefringent material are then passed through the analyzer, which is oriented to pass a polarized vibration direction perpendicular to that of the polarizer, hence, the analyzer passes only those components of the light rays that are parallel to the polarization direction of the analyzer. As one of the waves is retarded compared to the other, interference occurs between the waves as they pass through the analyzer. Therefore, bright colors can be seen when observed through crossed polarizers. The wax molecules inside my anisotropic wax disks are in the smectic phase at room temperature around 22ºC they are birefringent and can be observed under the polarized light microscope. In addition, polarized light microscope requires strain-free objectives and condensers to avoid depolarization effects on the transmitted light.

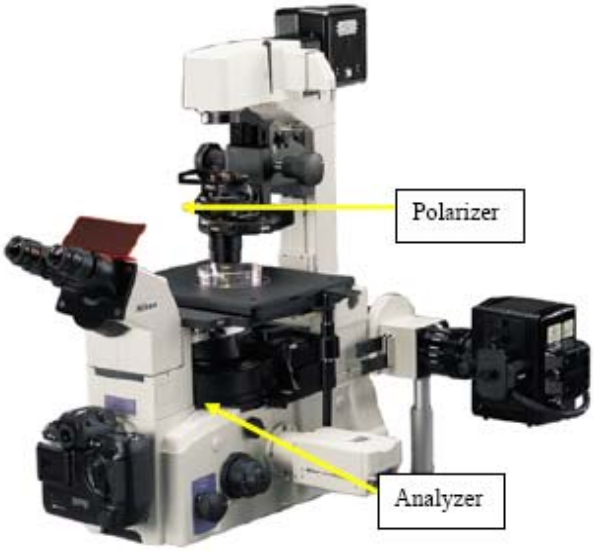

Picture taken from the Optical microscopy manual.

Figure 41. Polarized light microscope.

Inverted polarized light microscope (Nikon TE2000-U) used in our laboratory. A polarizer and an analyzer are installed in this microscope as shown by the yellow arrows.

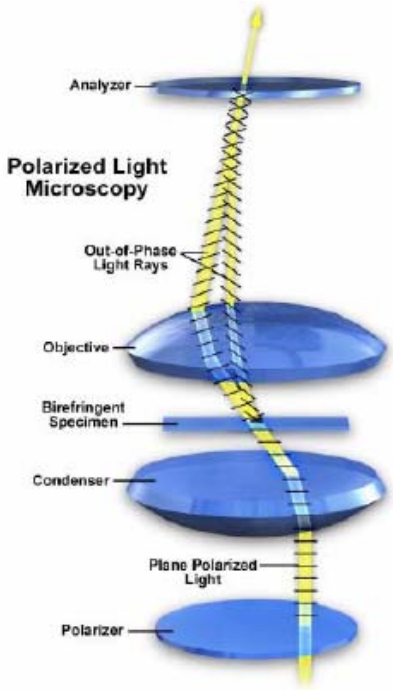

Figure taken from the Optical microscopy manual.

Figure 42. Sketch of the polarized light microscopy.

A systematic sketch of the polarized light microscopy.